

# Table of Contents

<b>Table of Contents</b>	<b>i</b>
<b>I Photo-excitation dynamics of alkalis</b>	<b>1</b>
<b>1 Introduction</b>	<b>3</b>
1.1 Imaging Excited-State Dynamics . . . . .	3
1.2 Desorption dynamics of RbHe-exciples . . . . .	4
1.3 Supervised work: potassium-doped nanodroplets . . . . .	5
<b>2 Results</b>	<b>7</b>
2.1 Imaging Excited-State Dynamics . . . . .	7
2.2 Desorption dynamics of RbHe exciples . . . . .	14
2.2.1 Time-resolved imaging spectroscopy . . . . .	14
2.2.2 Photoion imaging . . . . .	14
2.2.3 Photoelectron imaging . . . . .	17
2.3 TD-DFT dynamics simulation . . . . .	19
2.3.1 Direct ejection of bare Rb atoms from the $^2\Sigma_{1/2}$ and $^2\Pi_{1/2}$ -states . . . . .	19
2.3.2 RbHe exciplex formation around the $5p^2\Pi_{1/2}$ -state: non-radiative relaxation from the $5p^2\Pi_{3/2}$ -state . . .	21
<b>Bibliography</b>	<b>33</b>



## **Part I**

# **Photo-excitation dynamics of alkalis**



# Chapter 1

## Introduction

### 1.1 Imaging Excited-State Dynamics

**A**s mentioned in the introduction He nanodroplets capable of efficiently capturing and cooling atoms, molecules, and clusters for spectroscopy and dynamics studies[1,2]. So far, time-resolved experiments on He droplets doped with alkali (Ak) metal atoms were mostly focused on the formation of AkHe exciplexes induced by laser excitation[15-18,22,23]. The concurrent desorption of these excited species was estimated to proceed on a picosecond time scale[9,10,13,24-26]. This estimate, sufficient for studies employing nanosecond laser pulses, clearly lacks precision for experiments with sub-picosecond time resolution. Thus in the previous measurements as well as in experiments focusing on electronic and vibrational coherences of Ak atoms and molecules[17,19,22,23,27] the exact location of the dopants, attached to the droplets or in the vacuum, has remained somewhat uncertain.

Here we report a combined experimental and theoretical investigation of the excited-state dynamics of doped He nanodroplets in real time. The combination of fs pump-probe spectroscopy with velocity map imaging (VMI)[28] allows us to clearly disentangle complex formation, desorption, and ion solvation. As a model system, we investigate He droplets doped with single rubidium (Rb) atoms. Ground-state Rb atoms and small molecules are weakly bound to the He droplet surface in a dimple structure[29-31]. Therefore, the ejection dynamics of the excited Rb atom ( $Rb^*$ ) is not affected by processes such as the interaction of  $Rb^*$  with density waves traveling in the bulk of the droplet, as for  $Ag^*$ [11].

## 1.2 Desorption dynamics of RbHe-exciples

**U**NDERSTANDING the photochemistry of condensed phase systems and surfaces is essential in many research areas, such as atmospheric sciences[1] and photocatalysis[2]. However, complex diabatic couplings of electronic and motional degrees of freedom of various subunits of the system often present a major challenge. Moreover, the heterogeneity of multi-component solid or liquid systems and experimental difficulties in precisely preparing the sample and reproducing measurements tend to make it hard to unravel specific elementary reactions. In this respect, He nanodroplets doped with single atoms or well-defined complexes are ideal model systems for studying photodynamical processes in the condensed phase, both experimentally and theoretically. Due to their ultra-low temperature (0.37 K) and their quantum fluid nature, He nanodroplets have a homogeneous density distribution and dopant particles aggregate into cold clusters mostly inside the droplets[3,4]. Only alkali metal atoms and small clusters are attached to He droplets in loosely bound dimple-like states at the droplet surface[5-12].

While He nanodroplets are extremely inert and weakly-perturbing matrices for spectroscopy of embedded atoms and molecules in their electronic ground state, a rich photochemical dynamics is initiated upon electronic excitation or ionisation[13,14], involving electronic relaxation[15-18], the ejection of the dopant out of the droplet[19-26], chemical reactions within the dopant complex[27-29], and even among the dopant and the surrounding He[20,30-39].

As a general trend, electronically excited dopant atoms and small molecules tend to be ejected out of He droplets either as bare particles or with a few He atoms attached to them[15,40-42]. In particular, all atomic alkali species promptly desorb off the droplet surface, the only exceptions being Rb and Cs atoms in their lowest excited states[43,44]. The dynamics of the desorption process has recently been studied at an increasing level of detail[16,21,23,45], including time-resolved experiments and simulations[24,26]. The focus was on the competing processes of desorption of the dopant induced by laser excitation, and the dopant falling back into the He droplet upon photoionisation. The latter occurred at short pump-probe delay times when the distance between the photoion and the droplet was short enough for ion-He attraction to be effective.

The purpose of this work is to extend our joint experimental and theo-

retical study of the photodynamics of Rb-doped He nanodroplets to RbHe exciplexes[23,26]. The simultaneous effect of pairwise Rb-He attraction and repulsion of Rb from the He droplet as a whole results in an intricate dynamics, and interpretations have remained somewhat ambiguous with respect to the exciplex formation mechanism and time scale, as well as the origin of free exciplexes detached from the He droplets[16,26,30,33,34]. In particular the role of relaxation of internal degrees of freedom of the RbHe exciplex in the desorption process has not been explicitly addressed[46,47]. Here, we discuss in detail the interplay of the RbHe formation dynamics, the RbHe desorption off the He droplet surface, and the fall-back of  $[RbHe]^+$  created by photoionization in femtosecond pump-probe experiments[24,26,31]. We find that electronic spin-relaxation is the main process driving the desorption of RbHe off the He droplet.

### 1.3 Supervised work: potassium-doped nanodroplets

**U**NDER Nadine Halberstadt's and my supervision, a master stage – M2 *Physique Fondamentale* – titled “*Dynamics of a superfluid helium nanodroplet doped with a single potassium atom*” has been performed by Maxime Martinez.

The project investigates the static and dynamic behaviour of a single potassium atom excited from the  $K^-{}^4He_{1000}$  equilibrium configuration to the  $K^*(4p){}^4He_{1000}$  and  $K^*(5s){}^4He_{1000}$  states. The choice of potassium was motivated by a discrepancy in the time-resolved experimental studies<sup>[1-3]</sup>. Moreover, the mass of potassium sits between those of the heavier alkalis like rubidium and cesium, and the lighter ones, like lithium and sodium. Therefore, potassium presents an interesting case, being on the borderline between the classical regime for heavy alkalis and a quantum-mechanical regime for the lighter ones. Both treatments of the equilibrium properties and the  $5s \leftarrow 4s$  excitation are studied. This work is not included in the thesis but can be found here<sup>[4]</sup>.



# **Chapter 2**

## **Results**

### **2.1 Imaging Excited-State Dynamics**

## Imaging Excited-State Dynamics of Doped He Nanodroplets in Real-Time

Johannes von Vangerow,<sup>†</sup> Fran ois Coppens,<sup>‡</sup> Antonio Leal,<sup>§</sup> Marti Pi,<sup>§</sup> Manuel Barranco,<sup>§,‡</sup> Nadine Halberstadt,<sup>‡</sup> Frank Stienkemeier,<sup>†</sup> and Marcel Mudrich<sup>\*,†,¶</sup>

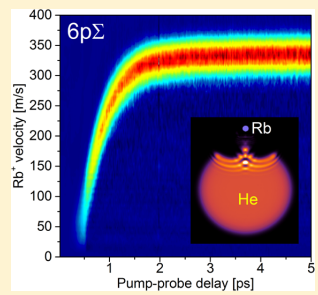
<sup>†</sup>Physikalisches Institut, Universit at Freiburg, Hermann-Herder-Str. 3, 79104 Freiburg, Germany

<sup>‡</sup>Laboratoire des Collisions, Agr gats, R activit , IRSAMC, UMR 5589, CNRS et Universit  Paul Sabatier-Toulouse 3, 118 route de Narbonne, F-31062 Toulouse Cedex 09, France

<sup>§</sup>Departament FQA, Facultat de F sica, and IN2UB, Universitat de Barcelona, Diagonal 645, 08028 Barcelona, Spain

### Supporting Information

**ABSTRACT:** The real-time dynamics of excited alkali metal atoms (Rb) attached to quantum fluid He nanodroplets is investigated using femtosecond imaging spectroscopy and time-dependent density functional theory. We disentangle the competing dynamics of desorption of excited Rb atoms off the He droplet surface and solvation inside the droplet interior as the Rb atom is ionized. For Rb excited to the 5p and 6p states, desorption occurs on starkly differing time scales ( $\sim 100$  versus  $\sim 1$  ps, respectively). The comparison between theory and experiment indicates that desorption proceeds either impulsively (6p) or in a transition regime between impulsive dissociation and complex desorption (5p).



He nanodroplets are intriguing quantum fluid objects of finite size capable of efficiently capturing and cooling atoms, molecules, and clusters for spectroscopy and dynamics studies.<sup>1,2</sup> Upon electronic excitation, embedded atoms and small molecules tend to move toward the droplet surface and may be ejected due to short-range electron-He repulsion.<sup>3</sup> In contrast, cations experience attractive forces toward the He droplets mediated by electrostatic polarization, which draw them to the droplet interior, where they may form snowball complexes.<sup>4–7</sup> These two opposing trends lead to a rich dynamics initiated by photoexcitation of embedded species involving desorption, electronic relaxation, complex formation, as well as solvation and desolvation of the ionized impurity. Similar dynamics have been observed when exciting pure He droplets with extreme-ultraviolet radiation<sup>20</sup> as well as for other types of clusters.<sup>21</sup>

So far, time-resolved experiments on He droplets doped with alkali (Ak) metal atoms were mostly focused on the formation of AkHe exciplexes induced by laser excitation.<sup>15–18,22,23</sup> The concurrent desorption of these excited species was estimated to proceed on a picosecond time scale.<sup>9,10,13,24–26</sup> This estimate, sufficient for studies employing nanosecond laser pulses, clearly lacks precision for experiments with sub-picosecond time resolution. Thus in the previous measurements as well as in experiments focusing on electronic and vibrational coherences of Ak atoms and molecules<sup>17,19,22,23,27</sup> the exact location of the dopants, attached to the droplets or in the vacuum, has remained somewhat uncertain.

Here we report a combined experimental and theoretical investigation of the excited-state dynamics of doped He nanodroplets in real time. The combination of fs pump-probe spectroscopy with velocity map imaging (VMI)<sup>28</sup> allows us to clearly disentangle complex formation, desorption, and ion solvation. As a model system, we investigate He droplets doped with single rubidium (Rb) atoms. Ground-state Rb atoms and small molecules are weakly bound to the He droplet surface in a dimple structure.<sup>29–31</sup> Therefore, the ejection dynamics of the excited Rb atom (Rb\*) is not affected by processes such as the interaction of Rb\* with density waves traveling in the bulk of the droplet, as for Ag\*.<sup>11</sup>

We excite droplet-bound Rb atoms to states correlating either to the lowest excited state 5p or to the higher lying state 6p. The dynamics is probed by ionizing Rb\* at variable delay times between photoexcitation ( $t = 0$ ) and photoionization ( $t = t_+$ ) while monitoring the velocity and signal yield of Rb<sup>+</sup> ions. A simulation based on time-dependent density functional theory (TDDFT) gives us insight into the time evolution both of Rb\* and of the Rb<sup>+</sup> ion taking into account the quantum fluid properties of the He environment. Using these techniques, we follow the trajectory of the excited and subsequently ionized Rb atom in detail as it escapes from the droplet surface or submerges into it. Although separated by only  $\sim 1.4$  eV in energy, the two states 5p and 6p are found to feature time

Received: November 6, 2016

Accepted: December 20, 2016

Published: December 20, 2016

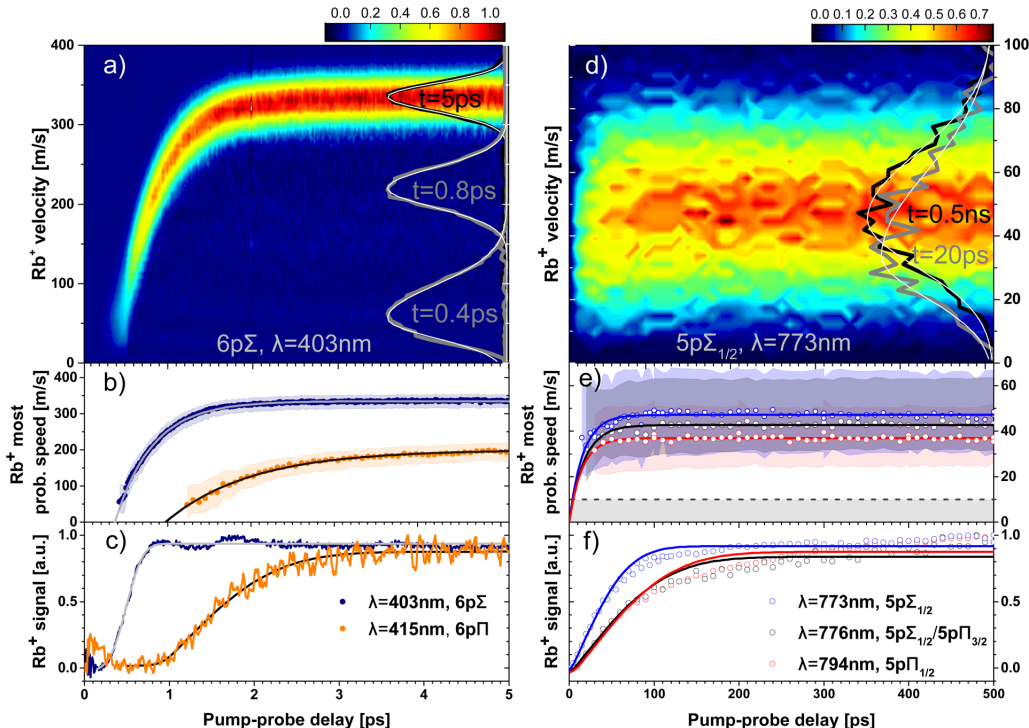


**Figure 1.**  $\text{Rb}^+$  transient speed distributions (a,d), most probable speeds (b,e), and ion yields (c,f) resulting from photoexcitation to He droplet perturbed states correlating to 6p (left column) and 5p states (right column) of Rb (pump) and subsequent ionization (probe). The shaded areas (b,e) indicate the left and right  $\epsilon^{-1/2}$  widths of the speed distributions. The shaded area at the bottom of panel e depicts the experimental resolution. The smooth lines are fits to the data (see text).

constants of the desorption dynamics differing by about 2 orders of magnitude.

Figure 1a,d shows examples of measured  $\text{Rb}^+$  transient speed distributions derived from the VMIs by angular integration. From these distributions we infer the most probable speeds (b,e) by fitting a skewed Gaussian distribution as illustrated by selected speed distributions shown on the right-hand sides of Figure 1a,d.<sup>34</sup> For the droplet perturbed Rb 6p states the most probable speeds (b) as well as the total  $\text{Rb}^+$  ion yields (c) show a steep rise within a few picoseconds. In contrast, for the droplet perturbed 5p states we record speed distributions (e) close to our experimental resolution of  $\sim 10 \text{ m/s}$  (shaded gray area) and ion yields (f) which increase within hundreds of picoseconds.

For the droplet perturbed Rb 6p excitations, the transient ion yield curves (c) have previously been interpreted in terms of the competing effects of repulsion from the He droplet surface and attraction of  $\text{Rb}^+$  toward it.<sup>14</sup> Accordingly, the slower dynamics of the 6pΠ state compared with that of the 6pΣ state is due to the weaker repulsion from the droplet. We term “fall-back time”,  $\tau_c$ , the critical delay discriminating between the ion falling back into the droplet and the ion escaping into the vacuum. It is obtained by fitting the 6p and 5p ion yield data with piecewisely defined asymmetric error function  $I(t) = A_0 + A \cdot \{[t \leq \mu] \sigma_- \cdot \text{erf}[(t - \mu)/\sigma_-] + [t > \mu] \sigma_+ \cdot \text{erf}[(t - \mu)/\sigma_+]\}$ , where  $\sigma_{\mp}$  denote widths on the right and left side of the inflection point  $\mu$ .  $\tau_c$  is obtained from computing the 50% rise time of that fit function. The evolution of the most probable

speeds  $\hat{v}$  is fitted by  $\hat{v}(t) = \hat{v}_f \{1 - \exp[-\ln 2 \cdot (t - t_0)/\tau]\}$ , from which we obtain the characteristic 50% rise times  $\tau_v = t_0 + \tau$ .

Note that for each applied pump–probe delay we measure the final velocity distribution of the ion after it has fully escaped from the droplet. Therefore, the experiment does not give direct access to the desorption dynamics of the neutral  $\text{Rb}^*$  atom. To get a complete picture of the dynamics, simulations based on the TDDFT approach are carried out using the functional of ref 35. Details of this approach have been described before.<sup>9,11,32</sup> In short, we consider droplets consisting of  $N = 1000$  atoms doped with one Rb atom. Because of its large mass compared with that of He we describe the dynamics of the Rb atom classically. The simulations of the full pump–probe sequence consist of two steps: the propagation of  $\text{Rb}^*$  in the excited state starting at  $t = 0$  (step 1) and the propagation of the  $\text{Rb}^+$  ion at times  $t > t_+$  (step 2). This is achieved by solving the coupled 3D TDDFT and Newton’s equations for the He droplet and the Rb impurity, respectively.

In step 1, the  $\text{Rb}^*$ –droplet interaction is obtained from the  $\text{Rb}^*$ –He  $n\Sigma$  and  $n\Pi$  pair potentials<sup>36</sup> with  $n = 5$  and 6, and includes the spin–orbit interaction in the usual He– $\text{Rb}^*$  distance-independent way; it also allows for the dynamic evolution of the internal electronic state of the  $\text{Rb}^*$  atom.<sup>11</sup> In step 2, the coupled dynamical equations are now simpler as they do not explicitly take into account the electronic structure of the closed-shell  $\text{Rb}^+$  ion. In all simulations, a spatial grid of 0.4 Å and a time step of 0.5 fs are used.

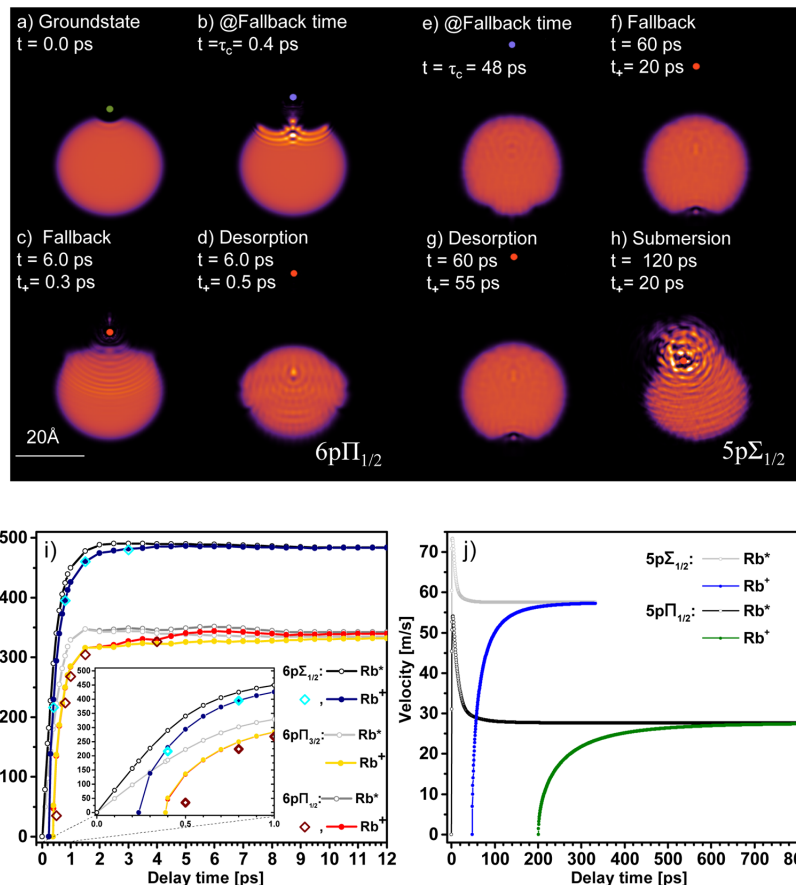


**Figure 2.** TDDFT-based 2D densities (a–d,e–h) and velocities (i,j) of Rb atoms attached to  $\text{He}_{1000}$  excited from equilibrium (a) to droplet perturbed 6p (left column) and 5p (right column) states. Configurations are shown for different propagation times  $t$  and ionization times  $t_+$ : (b,e) neutral Rb at fall-back time  $t = \tau_c$ ; (c,f)  $t_+ < \tau_c$  fall-back of  $\text{Rb}^+$  ion; (d,g)  $t_+ > \tau_c$ , desorption of  $\text{Rb}^+$ ; (h) solvation of  $\text{Rb}^+$ ; (i,j) evolution of  $\text{Rb}^*$  velocities with time  $t$  (gray open dots), and final velocities of  $\text{Rb}^+$  (colored filled dots) as a function of  $t_+$ .

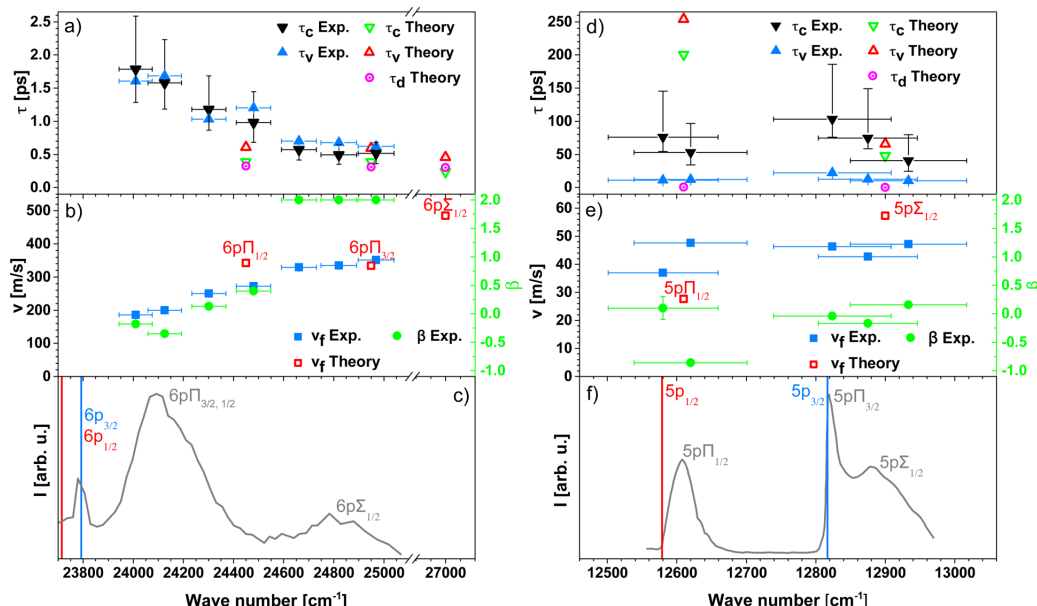
For step 1, initial conditions are given by the structure of the neutral  $\text{Rb}-\text{He}_{1000}$  complex in the ground state<sup>32</sup> obtained using the  $\text{Rb}-\text{He}$  potential of ref 37. For step 2 the initial conditions are given by the step 1 simulation at  $t = t_+$ . Carrying out the full simulations for step 2 is crucial for short and intermediate delays  $t_+ \lesssim \tau_c$  as the droplet is still far from being relaxed when  $\text{Rb}^*$  is photoionized. At variance, we have checked that keeping the droplet density frozen as done in ref 14 is a good approximation for long delays  $t_+ \gg \tau_c$ . In Figure 2i the open diamonds show the difference between carrying out the full simulation and keeping the He density frozen at  $t = \tau_c$  for  $t_+ \gtrsim \tau_c$  (filled dots). For illustration, these simulations are provided as animations in the Supporting Information.

Figure 2a–d,e–h shows snapshots of the resulting 2D densities for different propagation times  $t$  and ionization times  $t_+$  for the  $6p\Pi_{1/2}$  (left column) and  $5p\Sigma_{1/2}$  (right column) states. The ground-state dimple configuration is depicted in panel a. Figure 2b,e shows the configurations at the fall-back time  $\tau_c$ . Panels c, d and g, h illustrate the desorption and fall-back processes. When ionization occurs before the fall-back time,  $t_+ < \tau_c$  the ion turns around and submerges into the

droplet, where it becomes fully solvated (h). For  $t_+ > \tau_c$ , the ion keeps moving away from the droplet surface and fully desorbs (d, g). Panels i, j show the velocities of  $\text{Rb}^*$  (open symbols) and  $\text{Rb}^+$  ions (filled symbols). The inset shows a close-up of the 6p dynamics at short propagation times.

For the 6p states, the  $\text{Rb}^*$  velocity features a steep rise that levels out after  $\sim 2$  ps propagation time  $t$  (gray open dots). The final  $\text{Rb}^+$  velocity is reduced compared with the  $\text{Rb}^*$  velocity at short delays  $t_+ \lesssim 10$  ps (colored dots) due to the attraction of the  $\text{Rb}^+$  ion toward the He droplet. For long delays these values converge as the  $\text{Rb}^+-\text{He}$  droplet attraction drops off at large distances. For the 5p case, the  $\text{Rb}^*$  velocity shows an overshoot at short delays relative to the asymptotic value. This is due to the transient  $\text{Rb}^*-\text{He}$  droplet interaction being weakly attractive at intermediate distance, which slows down the ejected  $\text{Rb}^*$  atom. It derives from the  $\text{Rb}^*-\text{He}$  potentials featuring an outer attractive region.

A compilation of the time constants for fall-back,  $\tau_c$ , rise times of the ion speed,  $\tau_v$ , as well as most probable  $\text{Rb}^+$  final velocities,  $\hat{v}_f$  inferred from the experimental and theoretical data, is presented in Figure 3. The theory values of  $\tau_v$  are



**Figure 3.** Experimental and theoretical fall-back time constants  $\tau_c$  (a,d), velocity rise times  $\tau_v$  (a,d), theoretical Rb\* desorption times  $\tau_d$  (a,d), Rb<sup>+</sup> final most probable speeds  $v_f$  (b,e), and anisotropy parameters  $\beta$  (b,e) for different excitation wavenumbers corresponding to droplet perturbed Rb states 6p (left column) and 5p (right column). Panels c and f show fluorescence emission spectra as reference.<sup>25,38</sup> Vertical lines indicate free atomic transitions.

determined by fitting the final ion velocities using the same model as for the experimental data. In addition, Figure 3a,d contains desorption times  $\tau_d$  of the neutral Rb\* atoms inferred from the simulation by fitting the same model as for ion velocities. Note that for the 5p $\Pi_{1/2}$  and 5p $\Sigma_{1/2}$  states we obtain values  $\tau_d = 0.4$  and 0.2 ps, respectively, from the rising edges of the speed curves in Figure 2j. Figure 3b,e displays the anisotropy parameter  $\beta$  of the Rb<sup>+</sup> angular distributions measured at long delay times. For reference we include the corresponding fluorescence excitation spectra taken from literature.<sup>25,38</sup> Excitation wavenumbers for the theory values correspond to the peak positions of the simulated absorption spectra (not shown). Vertical error bars are connected to widths of the asymmetric fit function. Horizontal error bars reflect the spectral widths (FWHM) of the fs laser pulses.

The experimentally observed drastic difference between time scales for the 6p and 5p state dynamics is well-reproduced by the calculation. The general trend that fall-back times  $\tau_c$  decrease and final velocities rise as a function of excitation wavenumber reflects the increasing repulsion acting between Rb\* and the He droplet as the excitation energy is tuned up.<sup>9,13,24,26,32</sup> Fall-back times  $\tau_c$  and speed rise times  $\tau_v$  exceed the desorption times  $\tau_d$  of the neutral Rb\* atom because the range of Rb<sup>+</sup>-He attractive interaction is larger than that of Rb\*-He repulsion.<sup>14</sup>

Discrepancies are found for the asymptotic velocities of the 6p states that are smaller in the experiment than in the simulation by a factor of  $\sim 0.7$ . Accordingly, experimental fall-back and speed rise times exceed the simulated values by a factor of 2 for the 6p $\Sigma_{1/2}$  and up to a factor of 4 for the 6p $\Pi$  states. We attribute this mainly to the limited accuracy of the 6p $\Sigma$  and 6p $\Pi$  Rb\*-He pair potentials<sup>36</sup> used in the simulation, causing a substantial blue shift of the simulated 6p  $\leftarrow$  5s

absorption spectrum (not shown) with respect to the measured one.<sup>24,25</sup>

For the 5p states the fall-back times being considerably larger than the speed rise times indicates that the desorption dynamics deviates to some extent from the impulsive model. In the limit of statistical desorption of Rb\* atoms by an evaporation-like process, one would expect a continuously rising yield of free atoms and broad thermal distributions. Considering the slightly delayed, slow rise of the Rb<sup>+</sup> yield (Figure 1f) and the peaked but broadened speed distributions that feature only small up-shifts at short delays (Figures 1d,e), we conclude that the dynamics of 5p excited states proceeds in a transition regime from impulsive dissociation to more complex, evaporation-like desorption. This conclusion is supported by the anisotropy parameter  $\beta$  (Figure 3e), whose sign correctly indicates the symmetry of the dissociating complex<sup>9,13,24</sup> but whose absolute value is significantly reduced compared with that expected for impulsively dissociating complexes, in contrast with the 6p case (Figure 3b). Consequently, the quantitative agreement with the simulations, which do describe complex dynamical couplings within the superfluid model (Figure 2j) but do not contain statistical evaporation, is limited.

Aside from this, the experimentally observed higher final ion velocity and smaller fall-back time for the 5p $\Pi_{1/2}$  state compared with theory may be due to the measured signals being dominated by excitation of the blue edge of the 5p $\Pi_{1/2}$  feature. Considering the observed steep rise of fall-back time and drop of Rb<sup>+</sup> velocity toward the red edge of the 5p $\Pi_{1/2}$  feature, our results agree with the previous finding that Rb\* remains attached to the droplet surface upon narrow-band excitation at the red edge of the 5p $\Pi_{1/2}$  state.<sup>39,40</sup>

Excitation of the  $5p\Pi_{3/2}$  state leads to the formation of RbHe exciplexes because the Rb $^*$ -He pair interaction is strongly attractive in this state.<sup>15,16,38</sup> While exciplex formation is reproduced by the simulation, the ejection of exciplexes off the He droplet surface is not. However, we find that nonradiative relaxation to the  $5p\Pi_{1/2}$  state may supply enough kinetic energy to the Rb $^*$  atom to cause ejection. We therefore argue that when tuning the fs laser to the  $5p\Pi_{3/2}$  peak, the experimentally observed Rb $^+$  signal is mainly due to spin relaxation to the  $5p\Pi_{1/2}$  state.<sup>38</sup> Possibly the admixture of the nearby repulsive  $5p\Sigma_{1/2}$  state also contributes. The relaxation dynamics will be further studied using time-resolved photoelectron spectroscopy. Let us mention that the RbHe $^+$  pump–probe transients (not shown) closely follow the ones of Rb $^+$  but significantly differ from those previously measured using a one-color NIR scheme.<sup>15,22</sup> This raises some doubts as to the previous interpretation in terms of exciplex formation times and should be further investigated.

In conclusion, the observed dynamics of femtosecond pump–probe photoionization of Rb atoms attached to He nanodroplets is determined by the competition between the repulsive interaction of the droplet with the Rb atom in an excited state and the attractive interaction of the droplet with the Rb $^+$  cation, causing either desorption of Rb $^*$  off the droplet or submersion of the Rb $^+$  ion into the droplet interior, respectively. The resulting desorption dynamics proceeds impulsively within  $\sim 1$  ps for the 6p excited states and in a transition regime between impulsive dissociation and statistical desorption within  $\sim 100$  ps for the 5p states. This interplay between opposing trends (Rb $^*$  repulsion, Rb $^+$  attraction) is likely to be present in other types of clusters and condensed phase systems probed by time-resolved photoionization spectroscopy.

## ■ EXPERIMENTAL METHODS

The experimental setup has been previously described.<sup>14,32</sup> In brief, He droplets with an average diameter of 10 nm are created by continuous supersonic expansion and doped by one Rb atom on average.<sup>14,32</sup> The laser system generates amplified pulses of 100 fs duration at a repetition rate of 5 kHz with a tunable center wavelength in the near-infrared (NIR) region. Light in the visible range (VIS) is generated by frequency doubling. Pulses are split and separated in time in a Mach-Zehnder type interferometer. Droplet perturbed Rb 6p and 5p states are probed by one-color VIS and two-color NIR+VIS pump–probe schemes, respectively. NIR pulses are strongly attenuated to avoid excitations to higher lying states. Photoions are detected by a VMI spectrometer.<sup>24,28,32</sup> For varying pump–probe delay steps, mass-selected ion VMIs are recorded and inverse-Abel transformed.<sup>33</sup> For each pump–probe scheme, a background contribution from ionization of effusive Rb is observed. In the measurement probing the Rb 6p states, additional background arises from single pulse ionization. To extract the pump–probe correlated dynamics, these contributions are subtracted from the signal.

## ■ ASSOCIATED CONTENT

### Supporting Information

The following files are available free of charge. The Supporting Information is available free of charge on the ACS Publications website at DOI: [10.1021/acs.jpclett.6b02598](https://doi.org/10.1021/acs.jpclett.6b02598).

Desorption and fall-back dynamics of Rb atoms initially excited to the  $5p\Pi_{1/2}$  state and ionized at  $t_+ = 20$  ps. (AVI)

Desorption dynamics for  $5p\Pi_{1/2}$  excitation and  $t_+ = 55$  ps. (AVI)

Desorption and fall-back dynamics for  $6p\Pi_{1/2}$  excitation  $t_+ = 0.3$  ps. (AVI)

Desorption dynamics for  $6p\Pi_{1/2}$  excitation and  $t_+ = 0.5$  ps. (AVI)

## ■ AUTHOR INFORMATION

### Corresponding Author

\*E-mail: [mudrich@physik.uni-freiburg.de](mailto:mudrich@physik.uni-freiburg.de).

### ORCID

Marcel Mudrich: [0000-0003-4959-5220](https://orcid.org/0000-0003-4959-5220)

### Notes

The authors declare no competing financial interest.

## ■ ACKNOWLEDGMENTS

Financial support for this work by the Deutsche Forschungsgemeinschaft (grant nos. MU 2347/6-1 and IRTG 2079), DGI, Spain (grant no. FIS2014-52285-C2-1-P), and HPC resources from CALMIP (Grant P1039) is gratefully acknowledged. M.B. thanks the Université Féderale Toulouse Midi-Pyrénées for financial support through the “Chaires d’Attractivité 2014” program IMDYNHE.

## ■ REFERENCES

- Toennies, J. P.; Vilesov, A. F. *Angew. Chem., Int. Ed.* **2004**, *43*, 2622.
- Stienkemeier, F.; Lehmann, K. *J. Phys. B: At., Mol. Opt. Phys.* **2006**, *39*, R127.
- Brauer, N. B.; Smolarek, S.; Loginov, E.; Mateo, D.; Hernando, A.; Pi, M.; Barranco, M.; Buma, W. J.; Drabbels, M. *Phys. Rev. Lett.* **2013**, *111*, 153002.
- Tiggesbäumker, J.; Stienkemeier, F. *Phys. Chem. Chem. Phys.* **2007**, *9*, 4748–4770.
- Müller, S.; Mudrich, M.; Stienkemeier, F. *J. Chem. Phys.* **2009**, *131*, 044319.
- Theisen, M.; Lackner, F.; Ernst, W. E. *Phys. Chem. Chem. Phys.* **2010**, *12*, 14861–14863.
- Zhang, X.; Drabbels, M. *J. Chem. Phys.* **2012**, *137*, 051102.
- Smolarek, S.; Brauer, N. B.; Buma, W. J.; Drabbels, M. *J. Am. Chem. Soc.* **2010**, *132*, 14086–14091.
- Hernando, A.; Barranco, M.; Pi, M.; Loginov, E.; Langlet, M.; Drabbels, M. *Phys. Chem. Chem. Phys.* **2012**, *14*, 3996–4010.
- Loginov, E.; Drabbels, M. *J. Chem. Phys.* **2012**, *136*, 154302.
- Mateo, D.; Hernando, A.; Barranco, M.; Loginov, E.; Drabbels, M.; Pi, M. *Phys. Chem. Chem. Phys.* **2013**, *15*, 18388–18400.
- Leal, A.; Mateo, D.; Hernando, A.; Pi, M.; Barranco, M.; Ponti, A.; Cargnoni, F.; Drabbels, M. *Phys. Rev. B: Condens. Matter Mater. Phys.* **2014**, *90*, 224518.
- Loginov, E.; Hernando, A.; Beswick, J. A.; Halberstadt, N.; Drabbels, M. *J. Phys. Chem. A* **2015**, *119*, 6033–6044.
- von Vangerow, J.; John, O.; Stienkemeier, F.; Mudrich, M. *J. Chem. Phys.* **2015**, *143*, 034302.
- Droppelmann, G.; Bünermann, O.; Schulz, C. P.; Stienkemeier, F. *Phys. Rev. Lett.* **2004**, *93*, 0233402.
- Reho, J.; Higgins, J.; Lehmann, K. K.; Scoles, G. *J. Chem. Phys.* **2000**, *113*, 9694–9701.
- Mudrich, M.; Doppelmann, G.; Claas, P.; Schulz, C.; Stienkemeier, F. *Phys. Rev. Lett.* **2008**, *100*, 023401.
- Mudrich, M.; Stienkemeier, F. *Int. Rev. Phys. Chem.* **2014**, *33*, 301–339.

- (19) Bruder, L.; Mudrich, M.; Stienkemeier, F. *Phys. Chem. Chem. Phys.* **2015**, *17*, 23877–23885.
- (20) Ziemkiewicz, M. P.; Neumark, D. M.; Gessner, O. *Int. Rev. Phys. Chem.* **2015**, *34*, 239.
- (21) Masson, A.; Poisson, L.; Gaveau, M.-A.; Soep, B.; Mestdagh, J.-M.; Mazet, V.; Spiegelman, F. *J. Chem. Phys.* **2010**, *133*, 054307.
- (22) Schulz, C. P.; Claas, P.; Stienkemeier, F. *Phys. Rev. Lett.* **2001**, *87*, 153401.
- (23) Giese, C.; Mullins, T.; Grüner, B.; Weidemüller, M.; Stienkemeier, F.; Mudrich, M. *J. Chem. Phys.* **2012**, *137*, 244307.
- (24) Fechner, L.; Grüner, B.; Sieg, A.; Callegari, C.; Ancilotto, F.; Stienkemeier, F.; Mudrich, M. *Phys. Chem. Chem. Phys.* **2012**, *14*, 3843.
- (25) Piffrader, A.; Allard, O.; Auböck, G.; Callegari, C.; Ernst, W.; Huber, R.; Ancilotto, F. *J. Chem. Phys.* **2010**, *133*, 164502.
- (26) Loginov, E.; Drabbels, M. *J. Phys. Chem. A* **2014**, *118*, 2738–2748.
- (27) Grüner, B.; Schlesinger, M.; Heister, P.; Strunz, W. T.; Stienkemeier, F.; Mudrich, M. *Phys. Chem. Chem. Phys.* **2011**, *13*, 6816–6826.
- (28) Eppink, A. T. J. B.; Parker, D. H. *Rev. Sci. Instrum.* **1997**, *68*, 3477.
- (29) Ancilotto, F.; DeToffol, G.; Toigo, F. *Phys. Rev. B: Condens. Matter Mater. Phys.* **1995**, *52*, 16125–16129.
- (30) Stienkemeier, F.; Higgins, J.; Ernst, W. E.; Scoles, G. *Phys. Rev. Lett.* **1995**, *74*, 3592–3595.
- (31) Bünermann, O.; Droppeleman, G.; Hernando, A.; Mayol, R.; Stienkemeier, F. *J. Phys. Chem. A* **2007**, *111*, 12684.
- (32) von Vangerow, J.; Sieg, A.; Stienkemeier, F.; Mudrich, M.; Leal, A.; Mateo, D.; Hernando, A.; Barranco, M.; Pi, M. *J. Phys. Chem. A* **2014**, *118*, 6604–6614.
- (33) Dick, B. *Phys. Chem. Chem. Phys.* **2014**, *16*, 570–580.
- (34) Mudholkar, G. S.; Hutson, A. D. *J. Stat. Plan. Inference* **2000**, *83*, 291–309.
- (35) Ancilotto, F.; Barranco, M.; Caupin, F.; Mayol, R.; Pi, M. *Phys. Rev. B: Condens. Matter Mater. Phys.* **2005**, *72*, 214522.
- (36) Pascale, J. *Phys. Rev. A: At., Mol., Opt. Phys.* **1983**, *28*, 632–644.
- (37) Patil, S. H. *J. Chem. Phys.* **1991**, *94*, 8089–8095.
- (38) Brühl, F. R.; Trasca, R. A.; Ernst, W. E. *J. Chem. Phys.* **2001**, *115*, 10220–10224.
- (39) Auböck, G.; Nagl, J.; Callegari, C.; Ernst, W. E. *Phys. Rev. Lett.* **2008**, *101*, 035301.
- (40) Theisen, M.; Lackner, F.; Ernst, W. E. *J. Phys. Chem. A* **2011**, *115*, 7005–7009.

## 2.2 Desorption dynamics of RbHe exciplexes

### 2.2.1 Time-resolved imaging spectroscopy

Typical experimental total electron and  $[RbHe]^+$  ion VMIs recorded at a center wavelength of the pump laser pulse  $\lambda = 776$  nm and a pump-probe delay of 2 ns are shown in Figure ?? a) and c), respectively. In these VMIs, the laser polarization is oriented along the  $y$ -axis. The corresponding electron energy distribution and ion speed distribution inferred from these images are presented in Figure ?? b) and d), respectively. In addition, Figure ?? b) contains photoelectron spectra measured at  $\lambda = 773$  and at  $\lambda = 794$  nm. Note that the photoelectron spectra in Figure ?? b) are rescaled in terms of electron binding energies  $E_b = h\nu_2 - T_e$ , where  $h\nu_2 = 2hc/\lambda$  denotes the photon energy of the ionizing laser pulse and  $T_e$  is the measured electron kinetic energy. The dashed vertical lines represent  $E_b$  for free Rb atoms in their  $5p_{1/2}$  and  $5p_{3/2}$ -states.

### 2.2.2 Photoion imaging

The  $[RbHe]^+$  ion distribution [Figure ?? c)] is a round spot with a flat intensity distribution and a slight elongation in  $x$ -direction (perpendicular to the laser polarization). The corresponding speed distribution is broad and nearly symmetric. The red line depicts a skewed Gaussian distribution fitted to the data<sup>[5]</sup>. This fit is applied repeatedly to each speed distribution measured at various pump-probe delays in order to trace the evolution of the most probable kinetic energy, see Figure 2.1 a) and b). The yields of ions, shown in Figure 2.1 c) and d), are obtained by summing over ion counts contained in each image. Blue and red symbols show the results for  $Rb^+$  and  $[RbHe]^+$  ions, respectively. Both kinetic energies and ion yields monotonously increase within 100-500 ps, with a slight overshoot at  $\lambda = 773$  nm [Figure 2.1 a)]. This increase results from the competing processes of desorption of the excited neutral Rb and RbHe species, and falling back of the  $Rb^+$  and  $[RbHe]^+$  photoions into the He droplet due to attractive  $Rb^+$ -He interactions, as discussed in Refs.<sup>[6,7]</sup>. By comparing the experimental data with TD-DFT simulations, we concluded that the 5p-correlated states of Rb and RbHe desorb off He droplets not purely impulsively, but in a more complex evaporation-like process<sup>[7]</sup>. The overshoot of speeds in Figure 2.1 a) is likely due to weak long-range attractive forces acting between the desorbing Rb and RbHe and the He droplet surface, which slightly slow down the relative motion in the later stage of desorption.

The data in Figure 2.1 a) are measured at  $\lambda = 773$  nm ( $12937\text{ cm}^{-1}$ ),

which corresponds to the excitation of the RbHe complex into the  $5p\Sigma_{1/2}^-$ -state, with some contribution of the  $5p\Pi_{3/2}$ -state due to overlapping absorption bands and due to the broad spectral profile of the laser<sup>[8–10]</sup>. The  $5p\Sigma_{1/2}^-$ -state is the most repulsive one out of the three states studied here. Accordingly, the asymptotic most probable speed of  $\text{Rb}^+$  reached at long delays is comparatively high,  $\hat{v} = 85 \text{ m/s}$ , corresponding to a kinetic energy of  $8 \text{ cm}^{-1}$ , whereas for  $[\text{RbHe}]^+$  we find  $\hat{v} = 40 \text{ m/s}$  ( $5.8 \text{ cm}^{-1}$ ). Since the diatomic  $5p\Sigma_{1/2}^-$  RbHe potential is purely repulsive [Figure ?? a)], this component of the excited population results in the desorption of neat Rb atoms. Accordingly, the yield of detected  $\text{Rb}^+$  ions exceeds that of  $[\text{RbHe}]^+$  ions by about a factor 1.5.

At  $\lambda = 776 \text{ nm}$  ( $12887 \text{ cm}^{-1}$ ), a higher contribution of the  $5p\Pi_{3/2}$ -state is excited, which efficiently forms RbHe exciplexes<sup>[9]</sup>. Thus, the yield of  $[\text{RbHe}]^+$  ions is higher than that of  $\text{Rb}^+$  by a factor 1.5. The  $\text{Rb}^+$  and  $[\text{RbHe}]^+$  asymptotic most probable speed is  $\hat{v} = 42 \text{ m/s}$  ( $6.3 \text{ cm}^{-1}$ ), close to that of  $[\text{RbHe}]^+$  at  $\lambda = 773 \text{ nm}$ . At  $\lambda = 794 \text{ nm}$  ( $12595 \text{ cm}^{-1}$ ), the  $5p\Pi_{1/2}^-$ -state of the Rb-He droplet complex is excited (not shown), and no  $[\text{RbHe}]^+$  ions are detected. Therefore we have recorded only  $\text{Rb}^+$  ion images at that wavelength<sup>[7]</sup>. Here, the  $\text{Rb}^+$  asymptotic most probable speed is lowest,  $\hat{v} = 38 \text{ m/s}$  ( $5.1 \text{ cm}^{-1}$ ), because dopant-He repulsion is weaker.

The transient kinetic energies measured at all laser wavelengths rise within a delay time of about 500 ps. The characteristic energy rise time (to half value),  $\tau_E^i$ , and the asymptotic ion kinetic energy  $E_\infty^I$ , are determined by fitting the data with an exponential function

$$E^I(t) = E_\infty^I \cdot \left(1 - \exp[-\ln 2 \cdot t / \tau_E^i]\right). \quad (2.1)$$

The resulting fit parameters are summarized in table 2.1.

The ion yields increase with pump-probe delay slightly more slowly than the ion kinetic energies, where the  $\text{Rb}^+$  ion signal rises faster than the  $[\text{RbHe}]^+$  ion signal at short delays. The initial fast rise of the  $\text{Rb}^+$  ion yield flattens out at delays around 100 ps and continues to rise slightly up to about 2 ns. The  $[\text{RbHe}]^+$  ion yields show a similar initial fast rise followed by a more pronounced slow increase that levels off somewhat earlier. Therefore, for fitting the  $\text{Rb}^+$  and  $[\text{RbHe}]^+$  ion yield data we use a biexponential function,

$$I(t) = A_1^i \cdot \left(1 - \exp[-\ln 2 \cdot t / \tau_1^i]\right) + A_2^i \cdot \left(1 - \exp[-\ln 2 \cdot t / \tau_2^i]\right), \quad (2.2)$$

where  $(A_1^i, \tau_1^i)$  and  $(A_2^i, \tau_2^i)$  parametrize the fast and the slow signal rise, respectively.

$\lambda$ [nm]	State	Ion	$E_\infty^I$ [1/cm]	$\tau_E^i$ [ps]	$A_1^i$	$\tau_1^i$ [ps]	$A_2^i$	$\tau_2^i$ [ps]
773	$\Sigma_{1/2}/\Pi_{3/2}$	$\text{Rb}^+$	8.0(1)	17(1)	0.45(2)	32(1)	0.14(2)	234(33)
		$[\text{RbHe}]^+$	6.0(1)	10(2)	0.17(2)	41(6)	0.22(2)	178(17)
776	$\Pi_{3/2}/\Sigma_{1/2}$	$\text{Rb}^+$	6.5(3)	17(1)	0.24(2)	53(5)	0.16(2)	490(104)
		$[\text{RbHe}]^+$	6.6(3)	26(1)	0.60(1)	143(2)	0.00(1)	-
780	$\Pi_{3/2}$	$[\text{RbHe}]^+$	6.3(1)	24(2)	0.95(1)	186(1)	0.00(1)	-

Table 2.1: Time constants and energies inferred from pump-probe measurements of  $\text{Rb}^+$  and  $[\text{RbHe}]^+$  ion yields at the  $5\text{p}\Sigma_{1/2}$  and  $5\text{p}\Pi_{3/2}$ -states of the Rb-He droplet complex, obtained from fits with equations (2.1) and (2.2), see Figure 2.1.

While neither the  $\text{Rb}^+$  and  $[\text{RbHe}]^+$  asymptotic energies  $E_\infty^I$ , nor the energy rise times  $\tau_E^i$  depend much on  $\lambda$ , the rise times of ion yields of  $\text{RbHe}^+$ ,  $\tau_1^i$ , clearly decrease monotonically with decreasing  $\lambda$  (increasing photon energy) by a factor 6, ranging from 186 ps at  $\lambda = 780$  nm to 32 ps at  $\lambda = 773$  nm. The trend that the dynamics proceeds faster with decreasing  $\lambda$  (increasing photon energy) is partly due to the increasingly repulsive dopant-He interaction and agrees with our previous findings<sup>[6,7]</sup>. However, the observation that the ion yields rise more slowly than the ion kinetic energies cannot be understood with the concept of impulsive desorption and fall-back. In that model, ion kinetic energies should be affected by ion-He attraction up to long delay times exceeding the fall-back time. Note that in previous experiments on the Rb 6p-state, where desorption proceeded impulsively, ion energies indeed increased more slowly than ion yields<sup>[7]</sup>. Therefore we take our current finding ( $\tau_1^i, \tau_2^i > \tau_E^i$ ) as a further indication for a non-impulsive, evaporation-like desorption mechanism.

Furthermore, from our analysis of the VMIs we obtain information about the anisotropy of the ion angular distribution, characterized by the parameter  $\beta$ <sup>[11]</sup>. For  $[\text{RbHe}]^+$  at long delay times we find  $\beta = -0.39(1)$  when a higher contribution of the  $\Pi_{3/2}$ -state is excited at  $\lambda = 776$  nm. At  $\lambda = 773$  nm (mainly  $\Sigma_{1/2}$ -excitation), the anisotropy becomes slightly positive,  $\beta = 0.13(1)$ . The corresponding values for the  $\text{Rb}^+$  ion distributions are  $\beta = -0.16(1)$  and  $\beta = 0.17(1)$ , respectively. While the signs of the  $\beta$ -values are in accordance with the symmetries of the pseudo-diatom states (ideal perpendicular  $\Sigma \rightarrow \Pi$ -transition in a diatomic implies  $\beta = -1$ , parallel  $\Sigma \rightarrow \Sigma$ -transition implies  $\beta = 2$ ), the absolute values are much smaller. On the one hand, this is due to the mixing of excited  $\Sigma_{1/2}$  and  $\Pi_{3/2}$ -states.

On the other hand, the desorption process is significantly more complex than direct dissociation of a diatomic molecule. We recall that the  $\beta$ -values came much closer to the ideal values in the case of excitation of Rb to the high-lying 6p-correlated states, where desorption proceeded more impulsively<sup>[7,12,13]</sup>.

We mention that in earlier pump-probe experiments, significantly different Rb<sup>+</sup> and [RbHe]<sup>+</sup> ion yield curves were measured<sup>[14]</sup>. However, in those experiments, NIR light emitted directly from a mode-locked titanium:sapphire laser was used at a pulse repetition rate of 80 MHz. Therefore, a large fraction of the ion signals actually stemmed from Rb and RbHe that had been desorbed off the droplets by preceding pulse pairs. Thus, the observed pump-probe transients may have reflected the internal dynamics of free RbHe instead of the dynamics of the Rb-He droplet interaction. Besides, near-resonant two-photon excitation of higher lying states correlating to the Rb 5d-level were probably involved in the observed dynamics. This raises some doubts as to the conclusions of those previous experiments in terms of exciplex formation times<sup>[7,14]</sup>. Further studies are needed to clarify this issue.

From the overall resemblance of the [RbHe]<sup>+</sup> and Rb<sup>+</sup> kinetic energy curves and ion yields in the present study one is tempted to conclude that RbHe exciplex formation is fast and desorption of RbHe off the He droplet surface proceeds essentially in the same way as for neat Rb atoms. However, the more pronounced biexponential rise of [RbHe]<sup>+</sup> ion yields, as well as complementary delay-dependent photoelectron measurements, and numerical simulations presented in the following sections will show that the desorption dynamics of RbHe exciplexes actually is more complex than that of Rb atoms.

### 2.2.3 Photoelectron imaging

The photoelectron spectra recorded at the three characteristic laser wavelengths  $\lambda$  [Figure ?? b)] exhibit pronounced peaks around the Rb 5p<sub>1/2</sub> and 5p<sub>3/2</sub> atomic binding energies,  $E_{5p1/2}$  and  $E_{5p3/2}$ , respectively. Both the peak position and the peak width significantly vary with  $\lambda$ , as inferred from fits to the data with a Gaussian function, depicted as smooth lines. The resulting peak positions relative to  $E_{5p1/2}$  and  $E_{5p3/2}$  are plotted in Figure 2.2 a), b), respectively. Figure 2.2 c) shows the peak Gaussian widths  $\sigma$ . For reference, the open symbols represent the peak positions measured for the Rb atomic background. The scatter of data points around the literature value (grey horizontal line) indicates the level of precision of our measurements.

$\lambda$ [nm]	State	$E_1^e$ [1/cm]	$\tau_1^e$ [ps]	$E_2^e$ [1/cm]	$\tau_2^e$ [ps]	$E_\infty^e$ [1/cm]
773	$\Sigma_{1/2}/\Pi_{3/2}$	32(2)	15(2)	63(4)	683(130)	-53(5)
776	$\Pi_{3/2}/\Sigma_{1/2}$	36(2)	13(2)	110(4)	709(70)	-96(5)
794	$\Pi_{1/2}$	33(2)	-	-	-	-

Table 2.2: Time constants and energies inferred from fits of equation (2.3) to the transient photoelectron energies (Figure 2.2).

The excess energies for the  $5p\Sigma_{1/2}$  and  $5p\Pi_{3/2}$ -states,  $E_b - E_{5p1/2, 5p3/2}$  shown in Figure 2.2 b), exhibit a fast decay ( $E_1^e, \tau_1^e$ ) above and a slow decay ( $E_2^e, \tau_2^e$ ) below  $E_{5p3/2}$  (horizontal line at  $y = 0$ ). Therefore, these data are fitted with a biexponential decay function

$$E^e(t) = E_1^e \cdot \exp(-\ln 2 \cdot t/\tau_1^e) + E_2^e \cdot \exp(-\ln 2 \cdot t/\tau_2^e) + E_\infty^e. \quad (2.3)$$

Here,  $E_\infty^e$  denotes the asymptotic energy value at long delay times. When exciting the  $5p\Pi_{1/2}$ -state at  $\lambda = 794$  nm, the transient droplet correlated peak position remains constant within the experimental scatter. Therefore, merely the mean value  $E_1^e$  is determined. The resulting energies and time constants are summarized in table 2.2. The increasing peak widths in the cases of  $\lambda = 773$  and  $776$  nm are fitted by the simple exponential function given by Eq. (2.1).

The fact that the droplet-related photoelectron energy  $E_1^e$  for the  $\Pi_{1/2}$ -state is constant but shifted with respect to the atomic value indicates that most of the Rb atoms remain attached to the droplet surface upon electronic excitation, in accordance with previous studies<sup>[15,16]</sup>. Thus, the slowly rising  $Rb^+$ -ion signal measured at that wavelength, indicative for excited Rb desorption, reflects only a small fraction of Rb atoms, most of which actually remain bound to the droplets. The measured up-shift of electron energy of  $E_1^e = 33(2)$  cm<sup>-1</sup> is attributed to a lowering of the ionization threshold induced by the He environment. This value is in reasonable agreement with previous measurements, where the ionization threshold was found to be lowered by 50(10) cm<sup>-1</sup> at comparable conditions<sup>[16]</sup>.

The similar dynamics of electron energies and ion yields for the  $\Sigma_{1/2}$  and  $\Pi_{3/2}$ -states, a biexponential evolution with a fast component (tens of ps) and a slow component (hundreds of ps), are taken as a confirmation that two distinct relaxation processes occur simultaneously. The fast process – prompt desorption of excited Rb off the He droplet – is associated mainly with the  $\Sigma_{1/2}$ -component of the excited state, whereas the  $\Pi_{3/2}$ -component undergoes slow relaxation. The latter will be discussed in the following

sections. Deviations of the time constants  $\tau_1^i$  vs.  $\tau_1^e$ , and  $\tau_2^i$  vs.  $\tau_2^e$ , are mainly due to the different nature of the observables. Both ion yields and speeds are affected by the dynamics occurring *after* the probe-ionization, whereas electron spectra probe the electronic state (affected by the He configuration around the Rb) *at the moment* of ionization. In particular, ion signals provide information only about that fraction of ions that eventually detach from the He droplets, whereas electron signals are measured for all photoionization events, including those where the ion falls back into the droplet; in this respect the electron spectra are the better probes of the full dynamics, with the restriction that we cannot distinguish between the final products (Rb, RbHe, and Rb attached to a He droplet).

We mention that at  $\lambda = 776$  nm ( $\Pi_{3/2}$ -state), an extended low intensity distribution is present in the spectrum of Figure ?? b) at higher electron binding energies  $\geq 21,500$  cm<sup>-1</sup> (lower electron kinetic energies). We attribute this component to elastic scattering of photoelectrons with He atoms as they propagate through the He droplet. Low-energy features in photoelectron spectra due to electron-He scattering have been observed before, in particular when using one-photon ionization<sup>[17–20]</sup>. The fact that this feature is most pronounced for the  $\Pi_{3/2}$ -excitation may be related to the more abundant formation of RbHe exciplexes which enhances the electron-He scattering probability.

## 2.3 TD-DFT dynamics simulation

Time-dependent density functional theory (TD-DFT) simulations are carried out as thoroughly described in Refs.<sup>[21,22]</sup>. Starting with the Rb-droplet equilibrium configuration, the dynamics is initiated by a “vertical DFT transition” into the excited state. This is realized by suddenly switching from the potential energy surface of the Rb-He droplet ground state to that of the Rb-He excited state. The subsequent evolution of the system can be followed in real-time, as illustrated by the series of snapshots of the He density distribution (red area) and the position of the Rb atom (green and magenta dots) in Figure 2.3. Here, excitation of the  $5p\Pi_{3/2}$ -state at  $t = 0$  is followed by relaxation to the  $5p\Pi_{1/2}$ -state at  $t = 60$  ps.

### 2.3.1 Direct ejection of bare Rb atoms from the $^2\Sigma_{1/2}$ and $^2\Pi_{1/2}$ -states

From these data we now infer the relevant quantities to compare with the experimental results, such as the kinetic energy of the Rb atom relative to

the droplet, the occurrence of He density attached to Rb which we identify with the formation of an exciplex, and the transient interaction energy of the neutral and ionized Rb atom with the surrounding He. The latter is related to the kinetic energy of a photoelectron created in a time-delayed photoionization process.

Figure 2.4 collects our results for the dynamics of the Rb atom excited to the droplet-perturbed states correlating to the atomic 5p-state. For the  $\Sigma_{1/2}$  and  $\Pi_{1/2}$ -states, the velocities (dashed lines) and kinetic energies (solid lines) feature a rapid increase to reach a maximum at time  $t = 2\text{-}5$  ps after excitation, followed by a drop due to long-range attractive forces acting on the desorbing Rb atom. The asymptotic values are reached for  $t > 50$  ps. When exciting the  $\Pi_{3/2}$ -state, the Rb-velocity features a damped oscillation around zero indicating that the Rb atom remains bound to the He droplet surface. The following conclusions can be drawn from these results:

(i) Rb excited to the  $5p\Sigma_{1/2}$ -state detaches from the droplet reaching an asymptotic kinetic energy of  $13\text{ cm}^{-1}$ . This value deviates from the experimental one ( $8.0\text{ cm}^{-1}$ ) due to contributions of  $\Pi_{3/2}$ -excitation to the experimental signal. Despite of the shallow local minima in the corresponding Rb-He droplet potential surface [?? c)], no binding of He density to the departing Rb atom occurs. This finding is in accordance with experiments<sup>[9,12,14]</sup>, where mostly free Rb atoms were detected following excitation at wavelengths  $\lambda < 774\text{ nm}$ .

(ii) Rb excited to the  $5p\Pi_{1/2}$ -state also detaches from the He droplet, but the asymptotic kinetic energy is much lower,  $2.8\text{ cm}^{-1}$ . This value again deviates from the experimental one ( $5.1\text{ cm}^{-1}$ ), but the trend that desorption of the less repulsive  $\Pi_{1/2}$ -state yields a lower energy than for the  $\Sigma_{1/2}$ -state is well reproduced. The potential well at short distance  $\sim 3\text{ \AA}$  would in principle support a stable RbHe exciplex. However, at the low temperature of the He droplet, exciplex formation is hindered by a potential barrier located at  $\sim 5\text{ \AA}$ , between the well and the range where the  $5p\Pi_{1/2}$ -state is populated by excitation from the  $5s\Sigma_{1/2}$ -ground state ( $7\text{ \AA}$ )<sup>[9,23,24]</sup>.

We recall that in previous experiments using narrow-band excitation of the low energy edge of the  $\Pi_{1/2}$ -resonance, it was observed that Rb and Cs dopants remained attached to the He droplet surface<sup>[15]</sup>. However, our simulations correspond to the excitation at the peak of the resonance, where free Rb atoms are also observed in the experiment. Thus, our simulations are not in conflict with the experimental findings. Note that Quantum Monte Carlo (QMC) calculations carried out for this state<sup>[25]</sup> yielded a weakly bound Rb in a shallow dimple. Had we carried out a

*static* DFT relaxation, we would also have found a bound structure, due to the shallow minimum on the Rb-He droplet potential surface. However, in the dynamical TD-DFT simulation this minimum is too shallow to retain the departing Rb atom.

(iii) In our simulation we find that Rb excited to the  $5p\Pi_{3/2}$ -state remains bound to the He droplet surface where it forms a RbHe exciplex. Figure ?? shows two deep barrierless potential wells at a Rb-He distance of about 3 Å. In the course of the dynamics, the Rb atom is drawn to the well close to the droplet surface, develops a RbHe exciplex that remains bound to it, and oscillates around an equilibrium position of  $\sim 3$  Å above the static equilibrium position at the dimple as shown in Figure 2.4. This result is in full agreement with static QMC calculations by Leino et al.<sup>[26]</sup>. Note that our simulations do not provide any indication that the vibrational motion of the RbHe exciplex structure leads to its desorption from the He droplet.

The dynamics of the exciplex formation process can be quantitatively represented by integrating over the He density within a spherical inclusion volume with radius  $r_{\text{incl}}$  around Rb. The result is shown in Figure 2.5. Thus, for  $r_{\text{incl}} = 5.7$  Å, which contains the entire localized He density at the Rb atom without including He density of the remaining droplet, we find a rise to 75 % of the final value at  $t = 20$  ps. For  $t > 60$  ps the He number density stabilizes close to 1, indicating the full evolution of a RbHe exciplex containing 1 He atom. This result is in good agreement with the formation time estimated using the tunneling model by Reho et al.<sup>[23]</sup> using model parameters inferred from the previous fs-ps pump-probe measurements (42 ps)<sup>[27]</sup>.

The finding that the RbHe exciplex remains attached to the He droplet is in apparent contradiction to experiments where the ejection of free Rb and RbHe was clearly observed<sup>[9,12,14]</sup>. Therefore, an additional mechanism must be active that induces the desorption of the RbHe molecule off the He droplet surface.

### 2.3.2 RbHe exciplex formation around the $5p^2\Pi_{1/2}$ -state: non-radiative relaxation from the $5p^2\Pi_{3/2}$ -state

In the gas phase, a RbHe exciplex can form in the  $5p\Pi_{1/2}$ -state if enough kinetic energy is provided by collisions such that the Rb can overcome the potential barrier<sup>[24]</sup>. Alternatively, collisions of a RbHe formed in the  $5p\Pi_{3/2}$ -state with another atom or complex might induce relaxation into a RbHe electronic state correlating to the Rb  $5p_{1/2}$ -state. In this case the barrier is circumvented by the relaxation process, as the potential wells

$\eta$ (%)	$v_\infty$ (m/s)	Kin. energy (cm <sup>-1</sup> )
5	bound	–
10	13.4	0.64
12.5	43.0	6.6
15	62.4	13.9
20	80.4	23.0

Table 2.3: Asymptotic velocity and kinetic energy of the ejected RbHe exciplex for various values of the fraction  $\eta$  of the  $5p\Pi_{3/2, 1/2}$ -energy spacing of  $165\text{ cm}^{-1}$ , which is converted into kinetic energy of Rb by relaxation from the  $5p\Pi_{3/2}$  into the  $5p\Pi_{1/2}$ -state. The calculations are carried out at a delay time  $\Delta t = 60\text{ ps}$  between photo-excitation and non-radiative de-excitation of the Rb atom.

for the two states  $\Pi_{3/2}$  and  $\Pi_{1/2}$  are at similar Rb-He distances. In the condensed (droplet) phase at 0.4 K temperature, none of these mechanisms are active to explain the formation of RbHe  $5p^2\Pi_{1/2}$  exciplexes and their potential ejection.

However, Figure ?? a) indicates another possible mechanism: Non-radiative de-excitation from the  $5p\Pi_{3/2}$  to the  $5p\Pi_{1/2}$ -state accompanied by transfer of energy into the relative motion of the Rb atom away from the He droplet. Notice from the figure that the minimum of the  $5p\Pi_{3/2}$ -potential is at  $\sim 12683\text{ cm}^{-1}$ , and that of the  $5p\Pi_{1/2}$ -potential is at  $\sim 12518\text{ cm}^{-1}$ ; the value of this potential at the barrier is  $12611\text{ cm}^{-1}$ . Thus, non-radiative de-excitation of the Rb atom may add to its original kinetic energy a fraction of this  $165\text{ cm}^{-1}$  difference energy. Consequently, the RbHe exciplex will be ejected in the  $5p\Pi_{1/2}$ -state, and not in the  $5p\Pi_{3/2}$ -state that was originally photo-excited. Non-radiative electronic relaxation induced by the He droplet has been observed for a number of metal atoms<sup>[12,28–33]</sup>. In particular, previous measurements of the dispersed fluorescence emitted upon excitation of Rb into the  $5p\Pi_{3/2}$ -state of the Rb-He droplet complex have evidenced large populations of free Rb atoms in the  $5p\Pi_{1/2}$ -state<sup>[9]</sup>. Efficient spin-relaxation of  $5p\Pi_{3/2}$ -excited Rb atoms can be rationalized by the large cross section for mixing of fine structure states in collisions of alkali metal atoms with He<sup>[34]</sup>. For low-temperature Rb-He collisions, the fine structure relaxation rate was found to be enhanced by the transient formation of a RbHe exciplex by orders of magnitude compared to binary Rb-He collisions<sup>[24]</sup>.

Here, we explore this scenario within TD-DFT. Starting from Rb in the  $5p\Pi_{3/2}$ -state, we induce a “vertical DFT transition” by suddenly switching

potential energy surfaces from  $5p\Pi_{3/2}$  to  $5p\Pi_{1/2}$ , imparting to the Rb a kinetic energy corresponding to a fraction  $\eta$  of the available non-radiative de-excitation energy. The time  $\Delta t$  elapsing between the vertical excitation and de-excitation has to be chosen as well; this time influences the degree of RbHe  $5p\Pi_{3/2}$  exciplex formation which, as we have seen, may require some tens of ps. The actual value of these inputs cannot be determined by the model itself.

In the following, we present results obtained from simulations using as input parameters the delay before relaxation  $\Delta t = 60$  ps, and several values of  $\eta$ . As shown in Figure 2.4 (see also the bottom left panel of Figure 2.3), this –arbitrary– time is sufficient to allow for a full development of the  $5p\Pi_{3/2}$  RbHe exciplex and to bring it to a rather stationary configuration. Figure 2.3 shows snapshots of the evolution following the  $5s\Sigma_{1/2} \rightarrow 5p\Pi_{3/2} \rightarrow 5p\Pi_{1/2}$  process for  $\eta = 15\%$ ,  $\Delta t = 60$  ps. Thus, upon sudden relaxation to the  $5p\Pi_{1/2}$ -state, the RbHe structure promptly detaches from the remaining He droplet. The velocity of the Rb atom as a function of time is depicted in Figure 2.6 for this and other values of  $\eta$ . Clearly, as the fraction of relaxation energy converted to Rb kinetic energy is increased from 10 % to 15 %, the initial speed, and even more so, the asymptotic value for long evolution times rises significantly. Table 2.3 collects the results obtained for various values of  $\eta$ . It can be seen that a fairly small  $\eta \geq 10\%$  is enough to induce the ejection of the RbHe complex. For a value  $\eta = 12.5\%$ , the asymptotic value of the RbHe velocity matches best the experimental one measured for maximum  $5p\Pi_{3/2}$ -excitation at  $\lambda = 776$  nm.

When assuming that the relaxation-induced RbHe desorption proceeds as an impulsive dissociation reaction, the conversion factor  $\eta$  can be related to an effective mass of the He droplet,  $m_{eff}$ <sup>[35]</sup>. From  $\eta = 12.5\%$  we obtain  $m_{eff} = 12.7$  amu, which corresponds to about 3 He atoms effectively interacting with the excited RbHe. This value is significantly less than what was found for the prompt desorption of Rb and RbHe upon excitation of the Rb 6s and 6p-correlated states<sup>[12,13]</sup>. This is no surprise, though, since the orbital overlap between the excited RbHe and the He droplet is smaller than for the higher excited and more extended 6s and 6p-states. Besides, the effective mass model is not strictly valid in the present situation, since it neglects the internal degrees of freedom of RbHe which is taken as one fixed subunit.

Now that we have established the RbHe formation and desorption mechanisms, we can take our comparative study one step further and compute from the simulation results the electron binding energies to compare with the experimental photoelectron spectra. For this, we evaluate

the interaction energy of the excited Rb atom and of the Rb<sup>+</sup> ion with the droplet by calculating, respectively,

$$U^*(t) = \int d\mathbf{r} \mathcal{V}_{\text{He-Rb}^*}(|\mathbf{r} - \mathbf{r}_{\text{Rb}^*}|) \rho(\mathbf{r}, t) \quad (2.4)$$

and

$$U^+(t) = \int d\mathbf{r} \mathcal{V}_{\text{He-Rb}^+}(|\mathbf{r} - \mathbf{r}_{\text{Rb}^+}|) \rho(\mathbf{r}, t). \quad (2.5)$$

Here the He-Rb<sup>+</sup> pair potential  $\mathcal{V}_{\text{He-Rb}^+}$  is taken from Ref.<sup>[36]</sup>.

The interaction energies  $U^*(t)$  and  $U^+(t)$  are shown in Figure 2.7 for Rb in the  $\Sigma_{1/2}$ -state in a), for the  $\Pi_{1/2}$ -state in b), and for the  $\Pi_{3/2}$ -state in c). Figure 2.7 d) shows the evolution following the sudden relaxation of Rb to the  $\Pi_{1/2}$ -state at  $t = 60$  ps. The prompt desorption of Rb in the  $\Sigma_{1/2}$  and  $\Pi_{1/2}$ -states is seen as a sudden drop of  $U^*(t)$  near  $t = 0$  followed by a slow rise towards zero due to long-range van der Waals attraction as Rb departs from the He droplet. Due to the purely attractive interaction of the Rb<sup>+</sup> ion with the He droplet,  $U^+(t)$  monotonically rises to zero. The exciplex formation dynamics in the  $\Pi_{3/2}$ -state is reflected by the irregular behavior of  $U^*(t)$  and  $U^+(t)$ , eventually stabilizing at  $t > 60$  ps at negative values, *i.e.* in a configuration where Rb is bound to the He droplet. Only when allowing for a sudden relaxation into the  $\Pi_{1/2}$ -state at  $t = 60$  ps, the RbHe exciplex receives a momentum “kick” and subsequently detaches from the He droplet, in spite of a rising  $U^*(t)$ . The asymptotic values of  $U^*$  and  $U^+$  are then given by the binding energy of the free RbHe exciplex configuration. The fast oscillations at  $t > 65$  ps indicate that RbHe keeps vibrating as it is ejected.

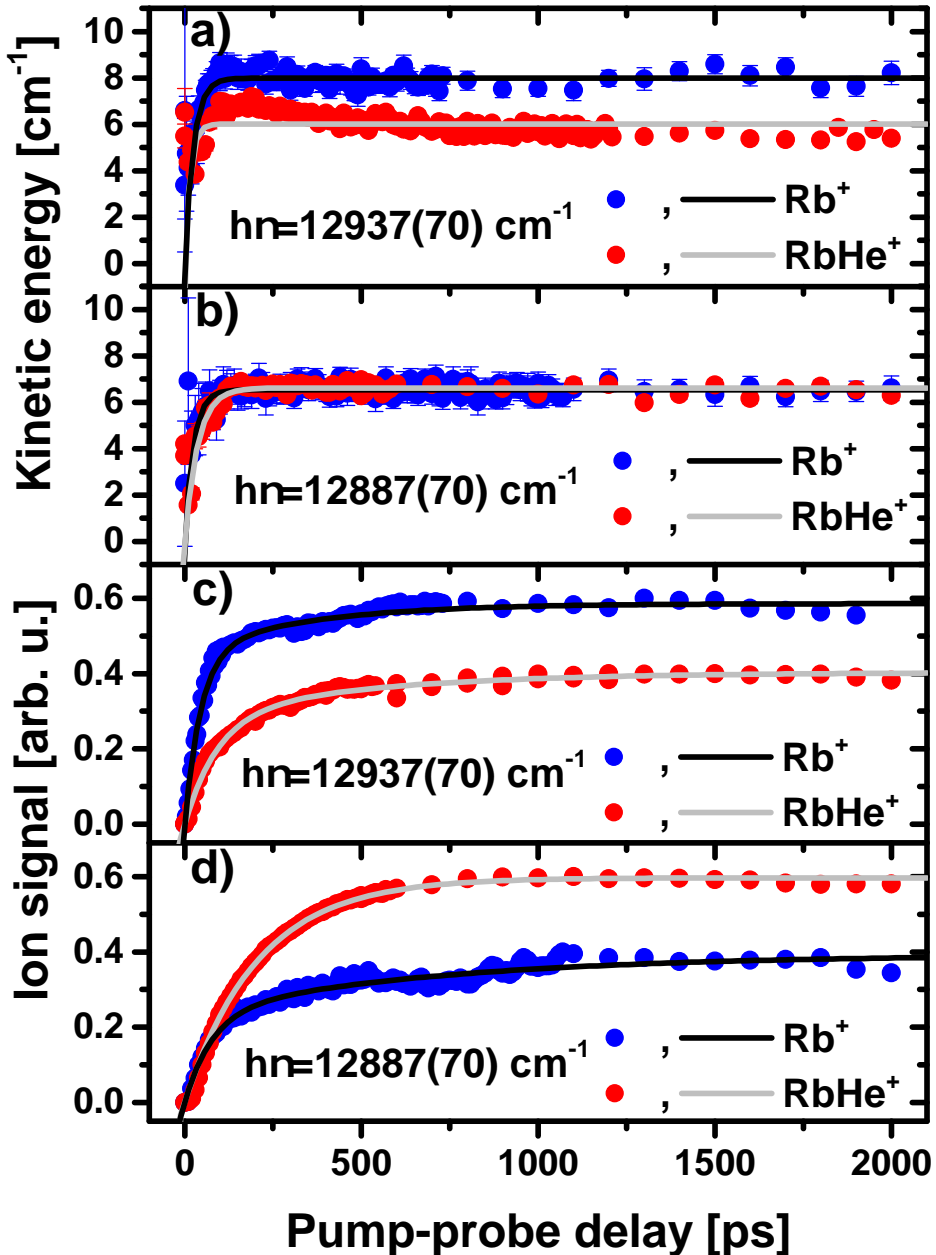


Figure 2.1: Rb<sup>+</sup> and [RbHe]<sup>+</sup> ion kinetic energies [a) and b)] and signal yields [c) and d)] recorded at laser wavelengths  $\lambda = 773$  nm [12937 cm<sup>-1</sup>, a) and c)] and  $\lambda = 776$  nm [12887 cm<sup>-1</sup>, b) and d)].

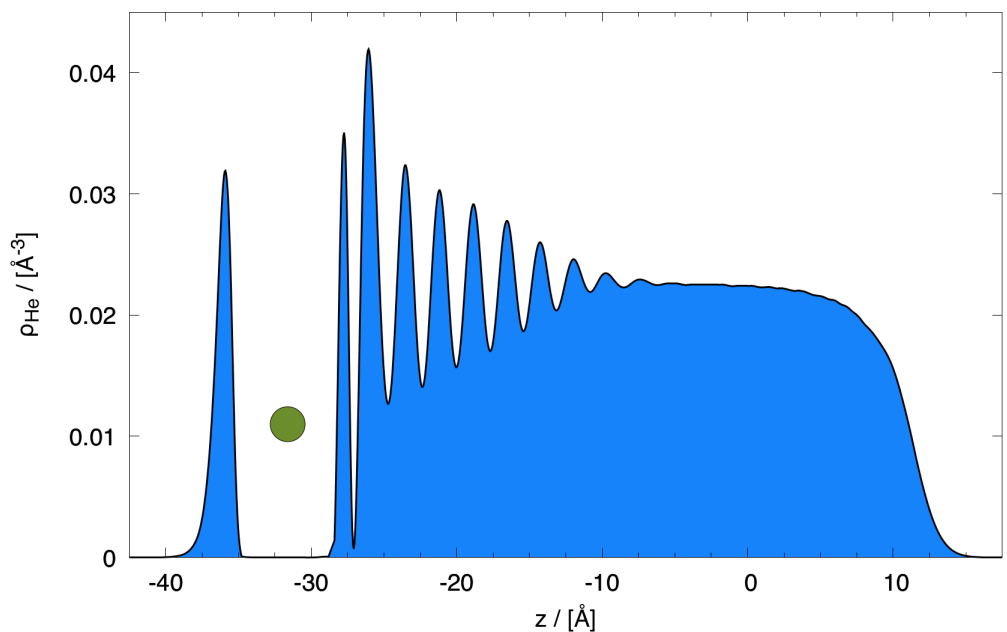


Figure 2.2: Photoelectron energies as a function of pump-probe delay (filled circles) recorded at laser wavelengths  $\lambda = 794$  nm ( $5p\Pi_{1/2}$ ) (a),  $\lambda = 773$  nm ( $5p\Sigma_{1/2}$ ), and  $\lambda = 776$  nm ( $5p\Pi_{3/2}$ ) (b). Open circles indicate the electron energies measured for atomic Rb background signal.

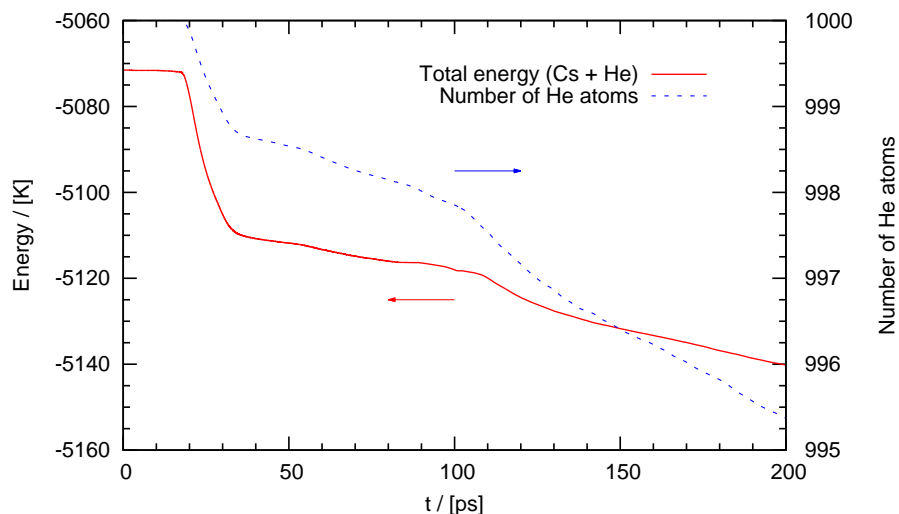


Figure 2.3: Snapshots of the He density during the evolution of the excited  $\text{RbHe}_{1000}$  complex for  $\eta = 15\%$ ,  $\Delta t = 60\text{ps}$ . The green dot represents the Rb atom excited into the  $5\text{p}\Pi_{3/2}$ -state; the magenta dot is the Rb atom after suddenly relaxing to the  $5\text{p}\Pi_{1/2}$ -state.

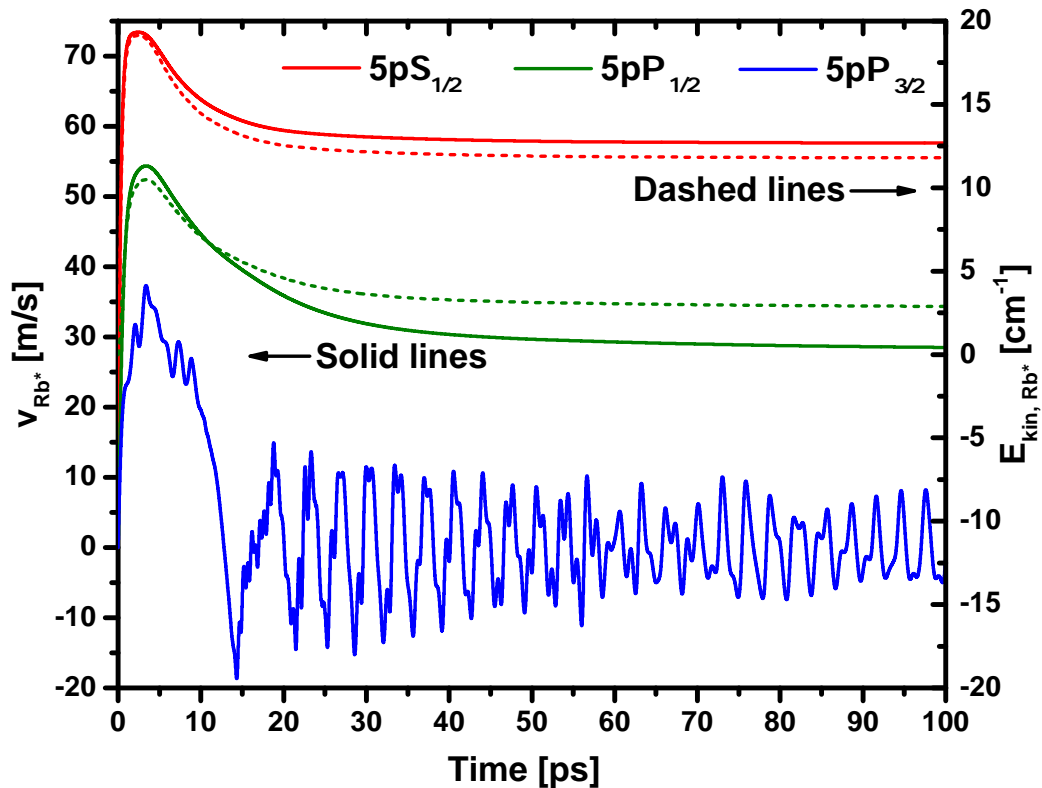


Figure 2.4: Velocity (solid lines, left scale) and kinetic energy (dashed lines, right scale) of the Rb atom excited to the 5p-state as a function of time. The kinetic energy of the  $5p\Pi_{3/2}$ -state is not given as this state remains bound to the droplet.

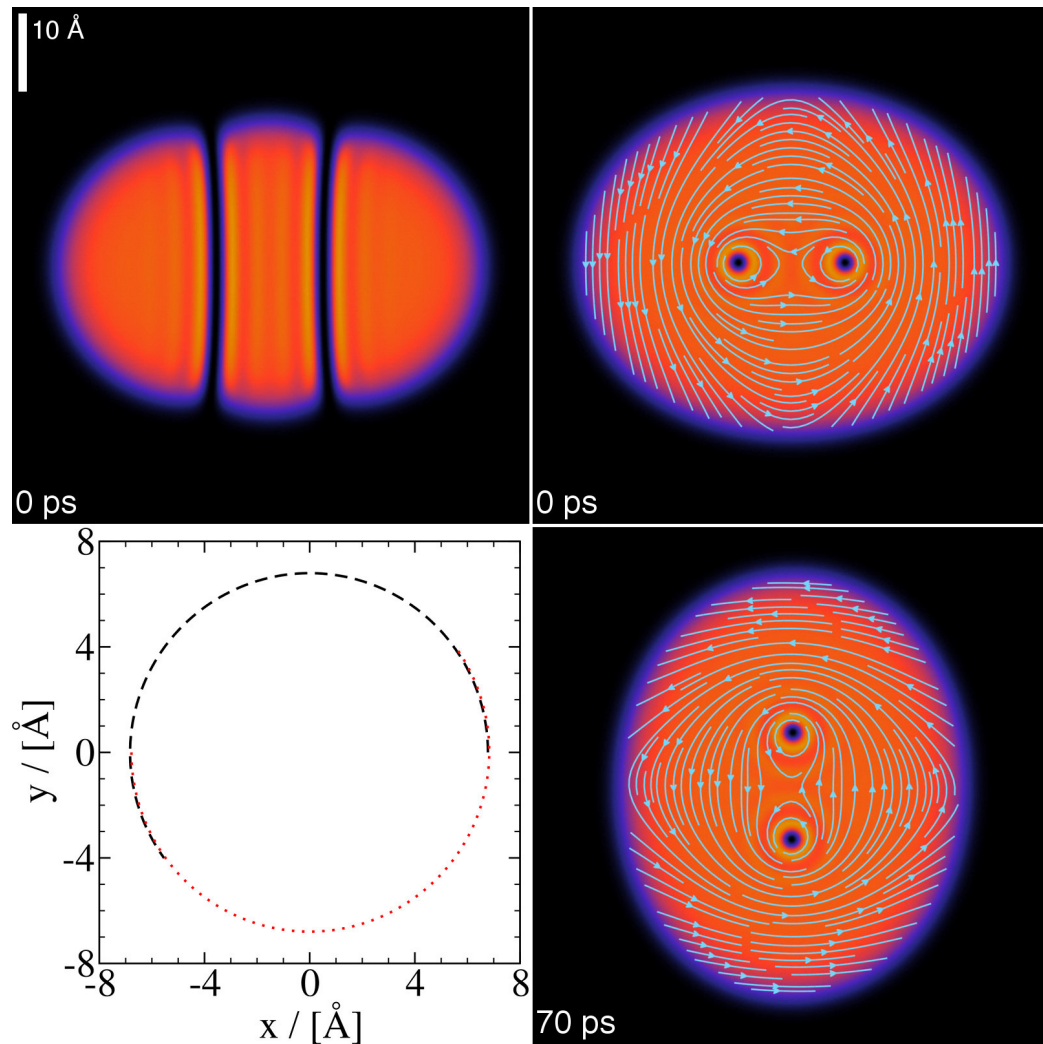


Figure 2.5: Simulated time evolution of the integrated He density within an inclusion volume of radius  $r_{incl} = 5.7 \text{ \AA}$  around the Rb atom excited to the  $5p\Pi_{3/2}$ -state.

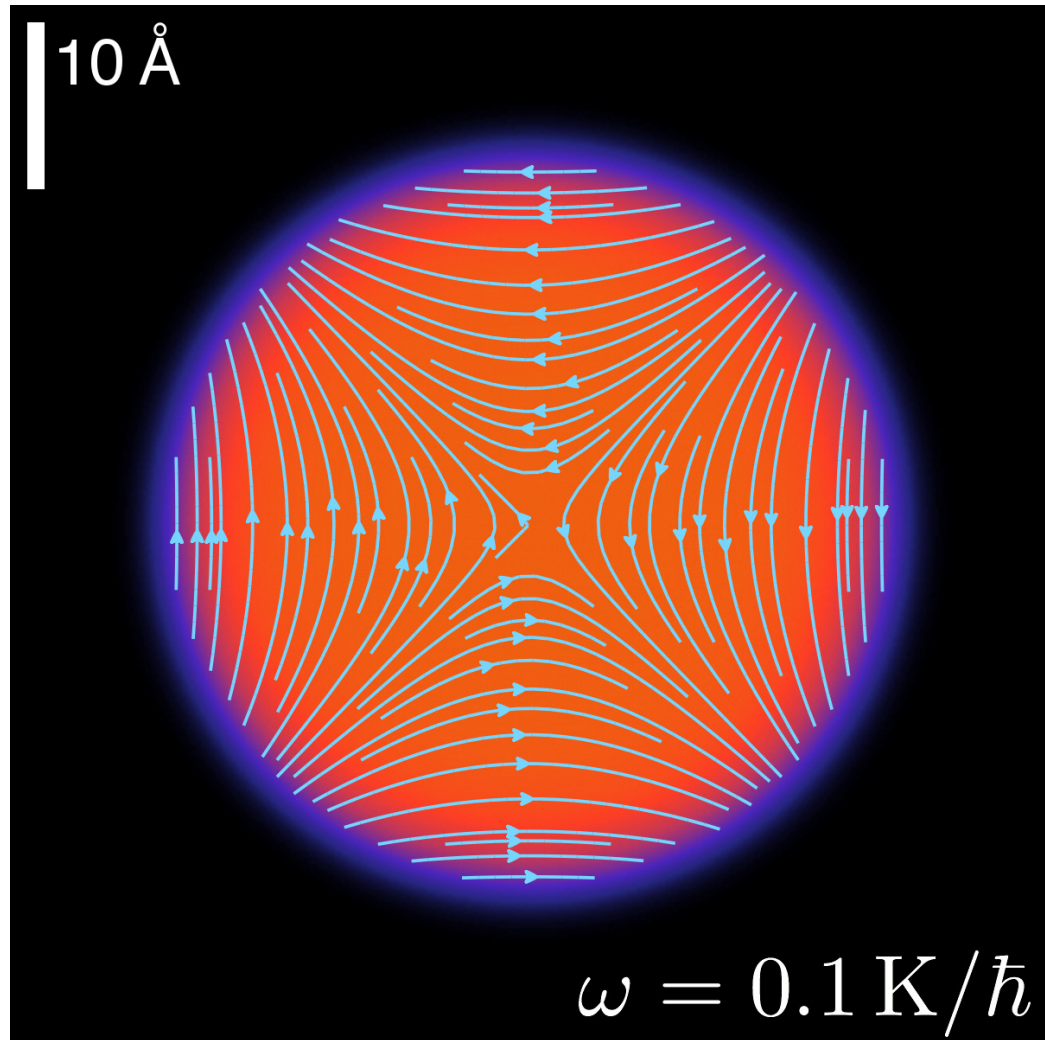
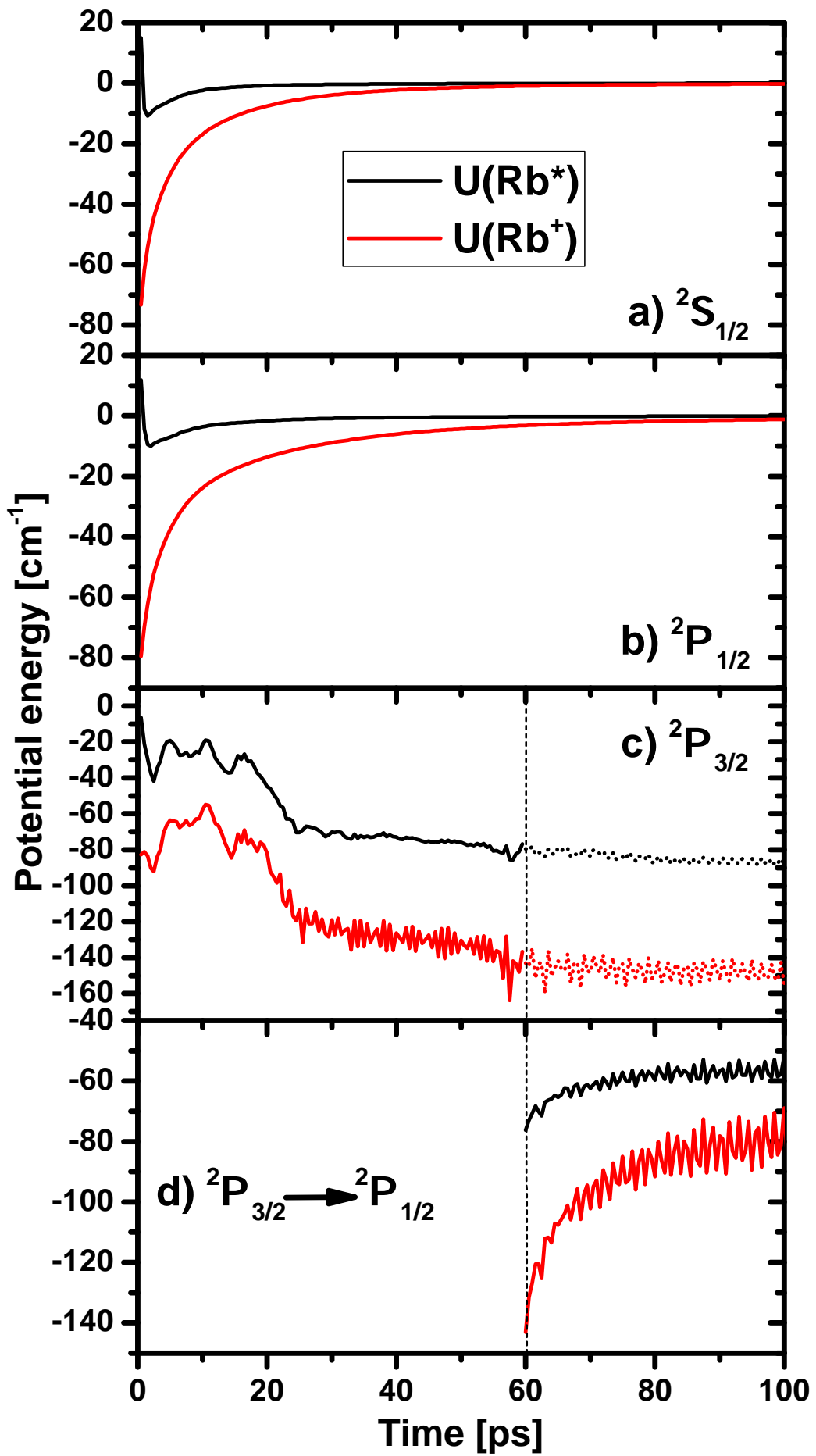
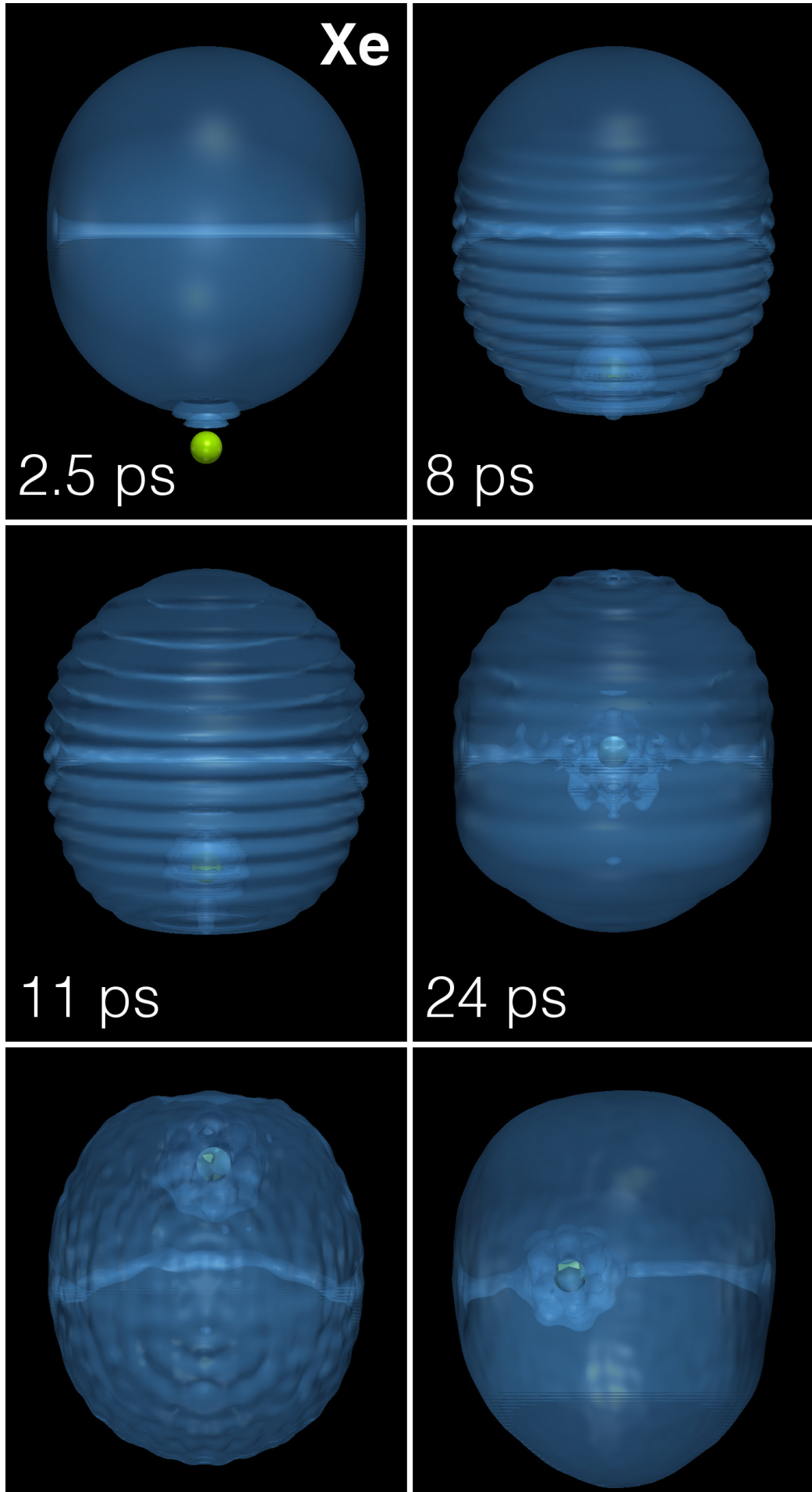


Figure 2.6: Velocity of the excited Rb atom with attached He density as a function of time after  $5p\Pi_{3/2} \rightarrow 5p\Pi_{1/2}$  relaxation at  $\Delta t = 60$  ps for various values of the energy conversion factor  $\eta$ .





# Bibliography

- [1] C. P. Schulz, P. Claas, and F. Stienkemeier, Phys. Rev. Lett. **87**, 153401 (2001), URL <https://link.aps.org/doi/10.1103/PhysRevLett.87.153401>.
- [2] J. Reho, J. Higgins, K. K. Lehmann, and G. Scoles, The Journal of Chemical Physics **113**, 9694 (2000), <https://doi.org/10.1063/1.1321034>, URL <https://doi.org/10.1063/1.1321034>.
- [3] J. Reho, J. Higgins, C. Callegari, K. K. Lehmann, and G. Scoles, The Journal of Chemical Physics **113**, 9686 (2000), <https://doi.org/10.1063/1.1321033>, URL <https://doi.org/10.1063/1.1321033>.
- [4] M. Martinez, Master's thesis, Université Toulouse III Paul Sabatier (2017), URL <https://github.com/bcntls2016/M2Report-MMartinez/blob/master/report/report.pdf>.
- [5] G. S. Mudholkar and A. D. Hutson, J. Stat. Plan. Inference **83**, 291 (2000).
- [6] J. von Vangerow, O. John, F. Stienkemeier, and M. Mudrich, J. Chem. Phys. **143**, 034302 (2015).
- [7] J. von Vangerow, F. Coppens, A. Leal, M. Pi, M. Barranco, N. Halberstadt, F. Stienkemeier, and M. Mudrich, J. Phys. Chem. Lett. **8**, 307 (2017).
- [8] F. Stienkemeier, J. Higgins, C. Callegari, S. I. Kanorsky, W. E. Ernst, and G. Scoles, Z. Phys. D **38**, 253 (1996).
- [9] F. R. Brühl, R. A. Trasca, and W. E. Ernst, J. Chem. Phys. **115**, 10220 (2001).
- [10] C. Callegari and F. Ancilotto, J. Phys. Chem. A **115**, 6789 (2011).
- [11] R. N. Zare, Mol. Photochem. **44**, 1 (1972).

- [12] L. Fechner, B. Grüner, A. Sieg, C. Callegari, F. Ancilotto, F. Stienkemeier, and M. Mudrich, *Phys. Chem. Chem. Phys.* **14**, 3843 (2012).
- [13] J. von Vangerow, A. Sieg, F. Stienkemeier, M. Mudrich, A. Leal, D. Mateo, A. Hernando, M. Barranco, and M. Pi, *J. Phys. Chem. A* **118**, 6604 (2014).
- [14] G. Dropplermann, O. Bünermann, C. P. Schulz, and F. Stienkemeier, *Phys. Rev. Lett.* **93**, 0233402 (2004).
- [15] G. Auböck, J. Nagl, C. Callegari, and W. E. Ernst, *Phys. Rev. Lett.* **101**, 035301 (2008).
- [16] M. Theisen, F. Lackner, G. Krois, and W. E. Ernst, *J. Phys. Chem. Lett.* **2**, 2778 (2011), <http://pubs.acs.org/doi/pdf/10.1021/jz201091v>, URL <http://pubs.acs.org/doi/abs/10.1021/jz201091v>.
- [17] E. Loginov, D. Rossi, and M. Drabbels, *Phys. Rev. Lett.* **95**, 163401 (2005).
- [18] D. S. Peterka, J. H. Kim, C. C. Wang, and D. M. Neumark, *J. Phys. Chem. B* **110**, 19945 (2006).
- [19] C. C. Wang, O. Kornilov, O. Gessner, J. H. Kim, D. S. Peterka, and D. M. Neumark, *J. Phys. Chem. A* **112**, 9356 (2008).
- [20] D. Buchta, S. R. Krishnan, N. B. Brauer, M. Drabbels, P. O'Keeffe, M. Devetta, M. Di Fraia, C. Callegari, R. Richter, M. Coreno, et al., *J. Phys. Chem. A* **117**, 4394 (2013).
- [21] D. Mateo, A. Hernando, M. Barranco, E. Loginov, M. Drabbels, and M. Pi, *Phys. Chem. Chem. Phys.* **15**, 18388 (2013), URL <http://dx.doi.org/10.1039/C3CP52221K>.
- [22] F. Ancilotto, M. Barranco, F. Coppens, J. Eloranta, N. Halberstadt, A. Hernando, D. Mateo, and M. Pi, *Int. Rev. Phys. Chem.* **36**, 621 (2017).
- [23] J. Reho, J. Higgins, C. Callegari, K. K. Lehmann, and G. Scoles, *J. Chem. Phys.* **113**, 9694 (2000).
- [24] K. Hirano, K. Enomoto, M. Kumakura, Y. Takahashi, and T. Yabuzaki, *Phys. Rev. A* **68**, 012722 (2003).
- [25] M. Leino, A. Viel, and R. E. Zillich, *J. Chem. Phys.* **129**, 184308 (2008).

- [26] M. Leino, A. Viel, and R. E. Zillich, *J. Chem. Phys.* **134**, 024316 (2011).
- [27] C. Giese, T. Mullins, B. Grüner, M. Weidemüller, F. Stienke-meier, and M. Mudrich, *J. Chem. Phys.* **137**, 244307 (2012), URL <http://scitation.aip.org/content/aip/journal/jcp/137/24/10.1063/1.4772749>.
- [28] E. Loginov and M. Drabbels, *J. Phys. Chem. A* **111**, 7504 (2007).
- [29] A. Kautsch, M. Koch, and W. E. Ernst, *J. Phys. Chem. A* **117**, 9621 (2013).
- [30] M. Koch, A. Kautsch, F. Lackner, and W. E. Ernst, *J. Phys. Chem. A* **118**, 8373 (2014).
- [31] F. Lindebner, A. Kautsch, M. Koch, and W. E. Ernst, *Int. J. Mass Spectrom.* **365-366**, 255 (2014), ISSN 1387-3806, URL <http://www.sciencedirect.com/science/article/pii/S1387380613004582>.
- [32] E. Loginov and M. Drabbels, *J. Phys. Chem. A* **118**, 2738 (2014), <http://pubs.acs.org/doi/pdf/10.1021/jp4121996>, URL <http://pubs.acs.org/doi/abs/10.1021/jp4121996>.
- [33] E. Loginov, A. Hernando, J. A. Beswick, N. Halberstadt, and M. Drabbels, *J. Phys. Chem. A* **119**, 6033 (2015), <http://dx.doi.org/10.1021/jp511885t>, URL <http://dx.doi.org/10.1021/jp511885t>.
- [34] L. Krause, *Adv. Chem. Phys.* (edited by J. W. McGowan (Wiley, New York), 1975).
- [35] A. Hernando, M. Barranco, M. Pi, E. Loginov, M. Langlet, and M. Drabbels, *Phys. Chem. Chem. Phys.* **14**, 3996 (2012).
- [36] A. Leal, D. Mateo, A. Hernando, M. Pi, M. Barranco, A. Ponti, F. Cargnoni, and M. Drabbels, *Phys. Rev. B* **90**, 224518 (2014), URL <http://link.aps.org/doi/10.1103/PhysRevB.90.224518>.